Voltage-dependent nanomechanical mapping at the solid−liquid interface

A research into the nanomechanical behaviour of gold electrodes in sulfuric acid using electrochemical atomic force microscopy

MASTER'S THESIS

Author:

J.H. Carstens BSc

5558816 — Experimental Physics — Utrecht University

Supervisors from the 3D Photovoltaics group, AMOLF:

Dr E. Allarcón Lladó

Dr M. Aarts

Examiners from Utrecht University,
from the Department of Physics and Astronomy:

Dr ir S. Faez

from the Debye Institute for Nanomaterials Science:

Dr I. Swart

12th May 2022

Abstract

Electrochemistry plays a role in green technologies such as catalysts, batteries, hydrogen production and photovoltaics. It is greatly influenced by local effects at the solid–liquid region, importantly electric double layers. Past research shows that atomic force microscopy is a suitable method for studying these inhomogeneous local effects. Our goal is to develop an experimental and data analysis method for studying these systems.

This thesis demonstrates EC-AFM measurements in PFT-mode, with a custom electrochemical cell filled with H_2SO_4 electrolyte, on a normal pulse voltammetry potential-controlled gold substrate. Data analysis of the force spectroscopy shows a clear dependency of the forces on the potential. Average force curves highlight the numerical values, and force curve maps show reproducible spatially inhomogeneous potential dependence of the adhesion. Deviations in the adhesion appear at potentials that are in literature associated with sulfate and oxide adsorption.

Contents

1 Introduction

As the world moves towards a sustainable future, the need for innovative green technologies remains high. Many of these – such as fuel cells [1], batteries [2], hydrogen production [3], and photovoltaics [4] – are greatly influenced by electrochemistry, 'the branch of chemistry concerned with the interrelation of electrical and chemical effects' (Bard & Faulkner [5]), both in the phenomenology and in the fabrication of these technologies. This is not surprising, since a key underlying challenge of sustainable innovations is the storage and conversion of, often electric, energy. In this thesis, I describe research at AMOLF into the combination of electrochemistry and atomic force microscopy.

Electrochemical (EC) processes are ones where electric current causes a chemical reaction or vice versa: a chemical reaction produces electricity. Usually, the chemical reactions are oxidation/reduction reactions occurring at an electrode-surface and the electric current is partially mediated by ion-migration in an electrolyte. Many macroscopic examples of these are well known, such as: corrosion[1], batteries, and electroplating (applying a metal coating to car parts, or gold plating a ring). To our interest, EC-processes are influenced greatly by surface features [7, 8] – whose description lies in the microscopic realm.

The structure and composition of a material surface can greatly influence the EC-behaviour. A striking example of this is the concept of single-atom catalysts [9, 10]. However, much about the different small-scale EC-processes is still unknown. Because of this, a tool is needed that can probe surfaces at the nanoscale – such as the atomic force microscope (AFM), a type of scanning probe microscope (SPM). An AFM 'sees' by 'feeling': much like a record player, it scans a surface with a nanoscale needle, or AFM tip, and the force on the needle images the surface. In § 3.3, I explain how an AFM works in more detail.

With the physics of an AFM, it is possible to investigate the region where the influence of surfaces on electrochemistry is found: the solid–liquid interface. And, because it has a scanning probe that can map a surface with nanoscale resolution (instead of similar techniques that measure interactions at a larger area, like the surface force apparatus), it can provide insight into the localised processes on inhomogeneous surfaces. The behaviour at this interface between electrode, electrolyte, and AFM tip is greatly influenced by the electric double layers (EDL) that form there – § 2.1 contains an explanation of the EDL. This region contains loosely bound ions, which are one of the sources of forces between the AFM tip and the surface, the others being van der Waals and Coulomb forces.

The AFM can investigate the forces at the phase boundary at a high frequency by collecting force–distance curves. From analysing these force curves, it is possible to extract various nanomechanical properties of the surface, such as: the adhesion [11, 12], elasticity, Young's modulus E [11], deformation and dissipation [13]. The AFM can be operated in different modes. In a classic method for spatially collecting nanomechanical information, force volume mapping, the AFM-probe is brought towards the surface at every point by linear ramping of the z-piezo. A more recent method is peak force tapping (PFT) [14–16], which executes force curves using sinusoidal actuation of the AFM-probe with frequencies up to 2 kHz, allowing for fast spatial mapping of the nanomechanical properties of the surface[2]. In literature, it has been shown that certain nanomechanical properties can be linked to the electrochemical state of a material. For example, Wang *et al.* [2] correlated the deformation of tungsten oxide by the AFM tip to the electrochemical potential applied to the surface using cyclic voltammetry, a common electrochemical experiment.

---

[1]Infrastructure operators apply an electric potential to underground pipes to prevent rust. This is called cathodic protection [6].

[2]A commercial name for PFT is quantitative nanomechanics (QNM) [15].

Noting that there are multiple EC-focused SPM techniques and with our interest in the heterogeneous nature of electrochemical processes in mind, we now take a look at such techniques. Firstly, scanning electrochemical microscopy (SECM) is an SPM technique where an 'ultramicroelectrode' measures current close to a surface [5]. This way, it spatially resolves electrochemical signals. However, the size of the electrode and mass transport of electrochemically active species limit the achievable resolution, and it is difficult to decouple the EC-data from topographical data. With the hybrid technique AFM-SECM, both are solved by using an AFM-probe as the electrode and keeping the distance with respect to the measured topography constant, using a double-pass scan [17]. Since the introduction of AFM-SECM in 2000, it has been extended to use PFT [11], and integrated commercial systems have been made available [18].

Another approach is kelvin probe force microscopy (KPFM). It works by applying a combined DC and AC potential between the AFM-tip and the surface, and detecting the electrostatic response force [19]. Due to the DC potential, conventional KPFM only works in air, but recent efforts have extended this method to electrolyte systems by using only an AC potential, enabling the mapping of the potential above a surface [20, 21]. Finally, the earlier mentioned AFM experiments can be performed *in-situ* in a three-electrode electrochemical cell, which is called electrochemical AFM (EC-AFM) [17], allowing full control over the EC-conditions of the system [12].

In this thesis, we aim to combine the electrochemical control of the surface and topographical mapping of EC-AFM with the acquisition of force–distance curves using PFT to simultaneously obtain the nanomechanical properties of the interface. This allows us to investigate the solid–liquid interface under varying electrochemical conditions and study the heterogeneous nature of EC-processes, which brings us to the main research questions that this thesis tries to answer:

1. Can the forces at and above the surface that a scanning probe microscope measures, in particular the adhesion, be related to the local electrochemical state of the potential-controlled surface?

2. Where in the force curve can the effects of electrochemistry be observed?

3. Can we use force spectroscopy to map the spatially inhomogeneous electrochemical processes *in-situ*?

We expect that the effects of electrochemical processes can be seen in the force curves, mostly close to the surface, because the constituent forces are influenced by them – double layer forces depend on the potential, and van der Waals forces depend on the material and its structure. As earlier mentioned, this has been shown in the past, for example for deformation [2]. We focus on the adhesion force because this is directly related to the work of adhesion, which – as shown in § 2.3 – contains information about all types of forces. However, rapid and spatially resolved mapping of the adhesion has only been recently possible [22], and as far as we know not that many electrochemistry-related studies have been done with it. Therefore, we think it is interesting to develop a method to spatially resolve force curves and adhesion at high speed under potential control. Ultimately, this would allow for non-invasive, spatially resolved, *in-situ* analysis of materials that are used in electrochemical applications, such as electrocatalysts.

The remainder of this thesis is structured in a standard way: after a theoretical background on the EDL and relevant forces, I explain the EC-AFM set-up, the fabrication of the gold-electrodes used as samples, and the voltammetry experiments. Then, I describe the data analysis method we developed, followed by the force spectroscopy results.

2 Theory and background

2.1 Electric double-layer

The electric double-layer (EDL) is a physical phenomenon that is important in describing the interactions between solids and liquids. It arises when a surface is introduced into a solution of ions[3]. As the name suggests, the EDL consists of two layers. The first layer is a tightly bound layer of oppositely charged ions with respect to the surface. These ions are tightly bound either electrostatically or by chemical processes that cause them to adsorb on the surface [5, 23]. As an example, in figure 1 it can be seen that on a surface with negative potential, the cations (positively charged ions) are adsorbed. Note that this image is a simplification. Due to the details of the adsorptivity of the ions with respect to a specific electrode material, it is also possible that some anions adsorb on the surface. This phenomenon is called 'charge reversal', and can also be caused by too many cations being adsorbed, requiring some anions to compensate those and achieve charge neutrality.
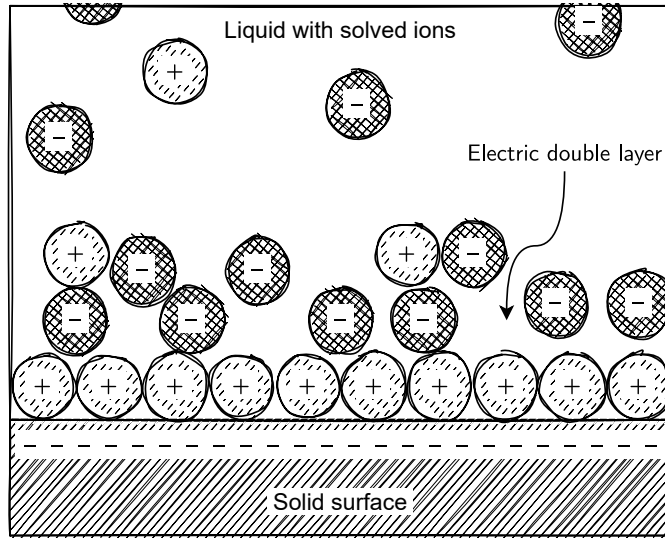
Figure 1 – Schematic figure of the EDL, in a situation where the surface is negatively charged, a layer of cations is adsorbed on the surface, and a diffuse layer of anions screens this first layer. This is a simple example, in reality, the EDL can look more complex.

The second layer is then formed by oppositely charged ions (in the example anions, or negatively charged ions) that form a more loosely bound layer where the electrostatic attraction of the ions to the layer below is balanced by their diffusive tendencies due to entropy. This layer has a concentration profile with a thickness of the order of a quantity called the Debye length, which is given by

$$\kappa^{-1} = \sqrt{\frac{\epsilon_r \epsilon_0 k_B T}{8\pi e^2 \rho_s}},\tag{1}$$

where κ is the inverse Debye length, e is the electron charge, ρ_s is the bulk ion concentration, ϵ_r is the relative permittivity, ϵ_0 is the vacuum permittivity, k_B is the Boltzmann constant and T is the temperature [24]. For water ($\epsilon_r = 80.2$ [25]) at room temperature ($T = 293.15\,\mathrm{K}$) the Debye length is given by the following expression:

$$\kappa^{-1}_{\text{water}} = \frac{0.305}{\sqrt{\rho_s}}\,\text{nm}.\tag{2}$$

Thus, the Debye length is inversely proportional to the ion concentration. For reference, in the following table typical values for the Debye length are shown:

---

[3]Interestingly, a similar double-layer phenomenon also occurs in plasma physics.

ρ_s (M)	κ^{-1} (nm)
0.001	9.644
0.01	3.050
0.1	0.964
1.0	0.305

Table 1 – Values for the Debye length κ^{-1} in nm for four monovalent ion concentrations in molar.

These expressions for the Debye length are found by analysis of the Poisson–Boltzmann (PB) equation, which forms a theoretical framework for describing the behaviour of charged surfaces and ions. The PB equation has the following form:

$$\frac{\mathrm{e}}{T}\frac{\mathrm{d}^2\psi(z)}{\mathrm{d}z^2} = \kappa^2 e^{\mathrm{e}/(\mathrm{k_B}T)}\sinh(\psi(z)). \tag{3}$$

Here, the electrostatic potential $\psi(z)$ at a distance z from a surface is described by a second-order differential equation, which can be solved when combined with appropriate boundary conditions. This theory assumes point-like monovalent ions, dissolved in a uniform medium.

Throughout scientific history, the theory of the EDL has been sharpened since its first description by Helmholtz [26], who realised that the charge in an electrode would be located at its surface and that there would be a counter charge in a solution which would also be located at the surface. Gouy and Chapman added to this picture that the potential and concentration profiles in the solution are exponential and that the layer becomes more diffuse further away from the surface. Finally, (but not definitive), Stern included the finite size of the ions into the model and the possibility for ions to adsorb on the surface, making the common model of the EDL the Gouy–Chapman–Stern (GCS) model. Specifically, the size of the ions limits the closest distance of approach to the surface of the first layer. This leads to the first layer being referred to as the Stern layer. Beyond this model, further effects that may play a role in EDLs are the finite size and dipole moment of the solvent molecules.

Another important force that is acting upon objects is the van der Waals (vdW)-force, which is attractive. By combining the repulsive forces due to EDLs with the attractive vdW force, one obtains a full picture of the forces on liquid-immersed solid objects as described by the commonly used DLVO[4]-theory. This sums itself up as $F_{\mathrm{DLVO}} = F_{\mathrm{EDL}} + F_{\mathrm{vdW}}$. DLVO-theory is obtained by solving the PB-equation, under the assumption of low potentials[5]. It thus is well applicable to for example colloids but less well to electrochemical systems where large potentials are applied.

2.2   Probe–surface forces

Because in this thesis an AFM is used to study forces near gold surfaces, it is useful to take a look at how these forces can be described theoretically. The forces between the AFM tip and the surface, while fundamentally all originating from the electromagnetic force, can be best described slightly more macroscopically: as a combination between electrostatic/EDL-forces and attractive vdW-forces. In simple terms, these two interactions have the following approximate form: $F_{\mathrm{vdW}}(D) \propto \frac{1}{D^2}$ and $F_{\mathrm{EDL}}(D) \propto e^{-\kappa D}$, where D is the separation between the tip and the sample. At low separations between the tip and the sample ($D <$

---

[4]Named after its developers, Derjaguin, Landau, Verwey and Overbeek.

[5]Low potentials, where the potential on a unit charge is lower than $\mathrm{k_B}T$, so there holds $|e\psi| < \mathrm{k_B}T$, allow for linearisation of the PB-equation (small-angle approximation), making it possible to find potentials for different geometries. This is called the Debye–Hückel approximation.

1 nm), a strong repulsive force acts because the electron orbitals at the edge of either object start to overlap. The Pauli exclusion principle is the main cause of this repulsion.

Firstly, the double-layer overlap force in an AFM-system in between the two double-layers surrounding the tip and the substrate can be modelled theoretically by solving the PB-equation for the system under consideration. Whereas DLVO-theory looks at interactions between two spheres, with low potentials, now a geometry must be used that is more accurate for this system, and varying potentials must be accounted for. In the book *Intermolecular and Surface Forces*, a derivation is given for the interaction between two double layers [27]. Without the need for a small potential approximation, and for a monovalent (1:1) electrolyte, by following an approach similar to Verwey and Overbeek [28], for various geometries, the potential is calculated. Regardless of geometry, these are all exponential expressions. For a sphere near a flat plane, which resembles an AFM-system the closest, the following force-expression is obtained as a function of distance D:

$$F_{\text{EDL}}(D) = \kappa R Z e^{-\kappa D}, \tag{4}$$

where κ^{-1} is the Debye length, R is the radius of the sphere, and Z is the coupling constant, of size

$$Z = 64\pi\epsilon_0\epsilon(k_B T/e)^2 \tanh^2(ze\psi_0/4k_B T). \tag{5}$$

Here, both surfaces are assumed to have the same constant potential ψ_0. This expression is accurate only for separations $D > \kappa^{-1}$; at lower separations numerical solutions of the PB-equation are required.

Secondly, the vdW-force for the system of interest can be modelled by integrating the intermolecular forces over the geometries of the objects. These intermolecular forces consist of a combination of London, Debye and Keesom forces, which are dispersion interactions between induced and/or permanent dipoles. The resultant interbody forces follow a power law that is dependent on the geometry. A simple approximation of intermolecular forces is the Lennard-Jones potential (LJ), which includes a positive term representing the Pauli-repulsion and a negative term representing the van der Waals-attraction – as the collective of negative intermolecular forces is commonly called the vdW-force. It has the following form:

$$V_{\text{LJ}}(D) = 4\epsilon\left[\left(\frac{\sigma}{D}\right)^{12} - \left(\frac{\sigma}{D}\right)^6\right], \tag{6}$$

where σ is the location of zero energy, and ϵ is the energy well-depth [29]. Taking the derivative yields the Lennard-Jones force – since this is a conservative force.

$$F_{\text{LJ}}(D) = -\frac{\text{d}V_{\text{LJ}}}{\text{d}D} \tag{7}$$

$$F_{\text{LJ}}(D) = \frac{24\epsilon}{D}\left[2\left(\frac{\sigma}{D}\right)^{12} - \left(\frac{\sigma}{D}\right)^6\right] \tag{8}$$

When approximating the AFM-system as a combination of a sphere and a surface, similarly to the double layer force, the following equation is given for the force between tip and sample [27, 30, 31]:

$$F_{\text{vdW}}(D) = -\frac{A_H R}{6D^2}, \tag{9}$$

where A_H is the Hamaker constant of the system. This constant depends on the material and indicates the strength of the interaction. In this thesis, a system consisting of a silicon–nitride (Si_3N_4) AFM-tip, immersed in a water-based solution and a gold surface is studied. To calculate the Hamaker constant between material i and j immersed in medium k, the following equation can be used [32]:

$$A_{ikj} \approx \left(\sqrt{A_{ii}} - \sqrt{A_{kk}}\right)\left(\sqrt{A_{jj}} - \sqrt{A_{kk}}\right), \tag{10}$$

where the individual terms are the Hamaker constant of the same-material interactions. For the combination of Si_3N_4 ($A_{ii} = 16.7 \times 10^{-20}$ J), water ($A_{kk} = 3.7 \times 10^{-20}$ J) and gold ($A_{jj} = 47.9 \times 10^{-20}$ J) [32] one obtains $A_H = 10.8 \times 10^{-20}$ J as the Hamaker constant.

To give an idea of what these forces look like, in figure 2, the above described relevant forces are plotted using equations (4) and (9), which both represent a sphere above a flat surface. The obtained total force[6] becomes:

$$F_{\text{total}}(D) = F_{\text{vdW}}(D) + F_{\text{EDL}}(D) = -R\left(\frac{A_H}{6D^2} + \kappa Z e^{-\kappa D}\right). \tag{11}$$

Here, parameters are used that represent the system of the experiments closely. This
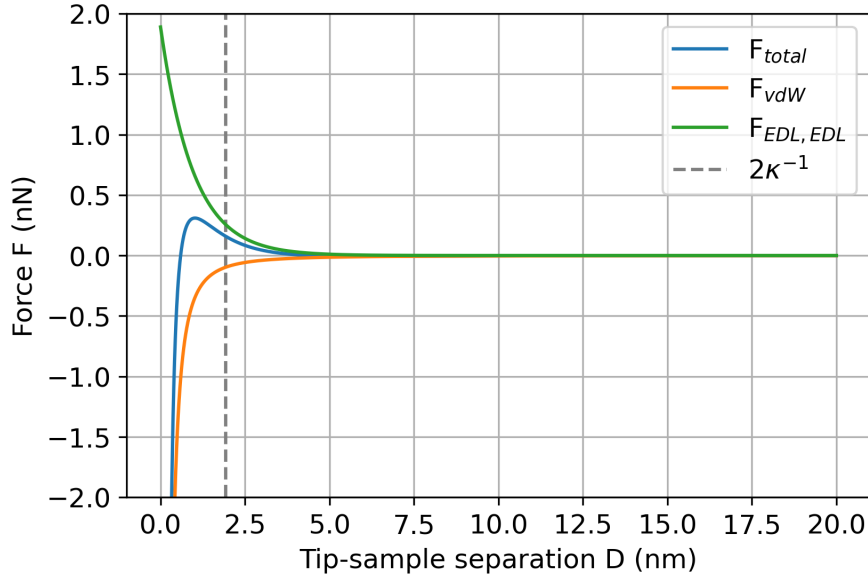
Figure 2 – Theoretical force profiles of equations (4) and (9) (green line and orange line) and their sum (blue line) between a Si_3N_4-sphere and an Au-surface immersed in water. The shown lines are for a 1:1 electrolyte at a concentration of 0.1 M with a sphere-radius of 20 nm at a potential of 1 V.

includes room temperature, a concentration of 0.1 mol, a Debye length of 0.96 nm, a tip/sphere-radius of 20 nm[7], a Hamaker constant of 10.8×10^{-20} J and a potential of 1 V.

The combination of the – in this case of comparable magnitude – attractive vdW-force and the repulsive EDL-force leads to a force profile with a maximum close to zero separation. Due to the small tip-radius, the forces are not more than several nN and do not extend much further than a separation of two Debye lengths (where the two double layers are more overlapping). Because both forces depend linearly on it, increasing the radius R will scale both forces equally to a magnitude where it is more significant at further separations. By varying the concentration, the EDL-force can be 'stretched' for lower concentrations or 'squeezed' for higher concentrations. The potential sets the height of the EDL-curve, which saturates at a potential of around 0.3 V, and by lowering the voltage flattens causing the total curve to be vdW-dominated.

For a more accurate expression for the tip–surface force, a more realistic tip-geometry than a sphere should be used, such as a cone [35]. Work by Siretanu *et al.* [36] and Zhao *et al.* [37] shows a method to compare theoretical force–distance curves to experimental

---

[6]Note that in this equation and figure, the repulsive force due to Pauli exclusion is not included – despite it greatly influencing the shape of a force curve – because it is not influenced by electrochemistry. Also, there is no simple model for this force in relevant conditions [27, 33], and the r^{-12}-term in the LJ-potential is not accurate.

[7]Corresponding to the tip-radius of a Bruker ScanAsyst Fluid tip [34].

data. They model the tip as a truncated cone with a flat end and compute EDL-forces by numerically solving the PB-equation. This method uses charge regulation to take the redistribution of surface charge and ions at close distances into account.

2.3   Adhesion

Adhesion – the attraction between two bodies in contact – is the nanomechanical property that this thesis focuses on. An AFM can measure the adhesion force. In a force curve, which looks similar to figure 3a, the adhesion force is the difference between the baseline and the minimum of the retrace curve.
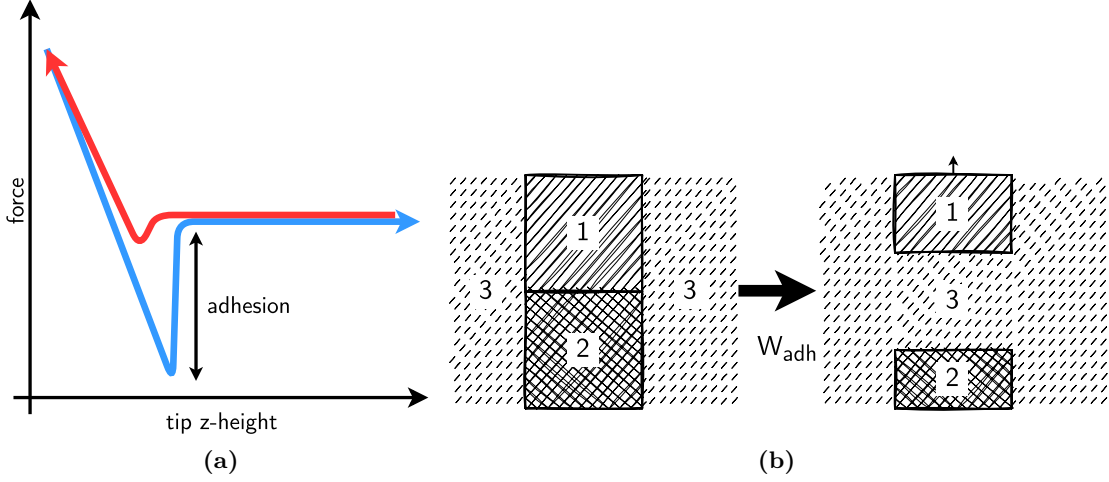
Figure 3 – (a) Sketch force–height curve, with the approach curve in red and the retract curve in blue, showing the adhesion (b) Definition of the work of adhesion W_{adh} for separating surface 1 and 2 in medium 3.

There are several contact-mechanics models that can be used for calculating the adhesion force, such as the Derjaguin–Muller–Toropov (DMT) model and the Johnson–Kendall–Roberts (JKR) model. Both models look at the forces between elastic surfaces, however, they apply to different systems. DMT theory works for stiff, low adhesion systems, and JKR theory works for more flexible, high-adhesion systems [30]. By fitting a retract-curve to the DMT model, the Young's modulus E can be obtained [15]. Moreover, the adhesion force can be related to the work of adhesion. For example, JKR theory provides the following formula [38, 39]:

$$F_{\mathrm{adh}} = -\frac{3}{2}\pi R_{\mathrm{T}} W_{\mathrm{adh}}, \tag{12}$$

where R_{T} is the tip radius of curvature.

The work of adhesion can be calculated theoretically for a material. Work is required to separate the tip and the sample. More generally, the work W_{132} of separating object 1 from object 2 immersed in substance 3, as figure 3b shows, is equal to the work required to separate surface 1 and 2, thereby creating two hypothetical surfaces 3, and bringing the 1 and 2 surfaces into contact with the 3 surfaces. In formula form, this looks as:

$$W_{132} = W_{12} + W_{33} - W_{13} - W_{23}, \tag{13}$$

where W_{ij} is the work to separate two surfaces of i and j [27]. Combining this equation with the Dupré equation, $\gamma_{ij} = \gamma_i + \gamma_j - W_{ij}$, or $W_{ij} = \gamma_i + \gamma_j - \gamma_{ij}$, and the identity $W_{ii} = 2\gamma_i$, yields:

$$W_{132} = \gamma_1 + \gamma_2 - \gamma_{12} + 2\gamma_3 - (\gamma_1 + \gamma_3 - \gamma_{13}) - (\gamma_2 + \gamma_3 - \gamma_{23}) \tag{14}$$

$$W_{132} = \gamma_{13} + \gamma_{23} - \gamma_{12}, \tag{15}$$

where γ_i is the surface energy of material i and γ_{ij} is the interfacial energy between material i and j. In other terms, the work of adhesion between tip (T) and surface (S) in a liquid (L) is given by:

$$W_{\mathrm{adh}} = \gamma_{\mathrm{SL}} + \gamma_{\mathrm{TL}} - \gamma_{\mathrm{TS}}. \tag{16}$$

Moreover, the work of adhesion can be a combination of vdW-, solvation, chemical, and EDL-forces [32], or in formula form: $W_{\mathrm{adh}} = W_{\mathrm{vdW}} + W_{\mathrm{solv}} + W_{\mathrm{chem}} + W_{\mathrm{EDL}}$. This implies that the work of adhesion, from the adhesion force using equation (12), can be used to measure changes in these properties.

2.4   Solid–liquid interface structure of gold in sulfuric acid

This thesis focuses on a system with a gold substrate immersed in an aqueous sulfuric acid solution. What is the electrochemical behaviour of such a system, and how are the ions structured? Three main processes (besides restructuring of the layer itself) can happen at the gold layer: double layer charging, sulfate adsorption, and oxide adsorption. These processes have been studied for Au(111) surfaces.

Firstly, research using cyclic voltammetry[8] reports that double layer charging happens from (all potentials are w.r.t. Ag/AgCl) -0.34 V to 0.53 V [40], where the lower bound is the onset of hydrogen evolution.

Secondly, sulfate (SO_4^{2-}) adsorption was reported to occur from 0.34 V to 0.84 V, with an increase in speed at 0.40 V (also the point of zero charge for the gold surface) [41]. The sulfates are reported to form an ordered layer beyond 0.90 V [39], or at 0.86 V in the increasing potential sweep, and to disorder at 0.84 V in the decreasing sweep [42].

Finally, gold oxidation, or oxide adsorption – this means that some kind of oxygen species are adsorbed on the surface, at higher potentials also forming gold oxides – is reported to occur at 1.20 V [43], at 1.15 V and 1.35 V [39], at 0.93 V–1.33 V [40], at 1.05 V and 1.3 V [42], and at 1.24 V–1.54 V [44]. The reverse process, oxide reduction, where the oxides are removed from the surface, is reported to occur between 0.80 V and 1.15 V [43], at 0.90 V [39], at 0.79 V [40], at 0.91 V [42], at 0.94 V [44] and at 0.86 V [45].

The detailed structure of the gold layer with its adsorbed ions can be measured using X-ray diffraction [41, 42], and can also be calculated with density functional theory (DFT) [37].

---

[8]See § 4.1.2 for an explanation of this technique.

3 Experimental set-up

In this chapter, the experimental setup that has been used is described. Mainly, it consists of an electrochemical cell that contains a gold-covered substrate, which is placed on the stage of an AFM (Bruker). A photograph of the set-up can be seen in figure 4. All electrodes of the electrochemical cell are connected to a potentiostat from *CH Instruments* (model CHI760E). The AFM head is lowered into the electrochemical cell to get close to the substrate. This allows for conducting AFM-experiments *in-situ* in a controlled electrochemical environment, which enables the simultaneous collection of AFM force-curves and electrochemical data. Consequently, this combination of techniques is often called EC-AFM (electrochemical AFM).
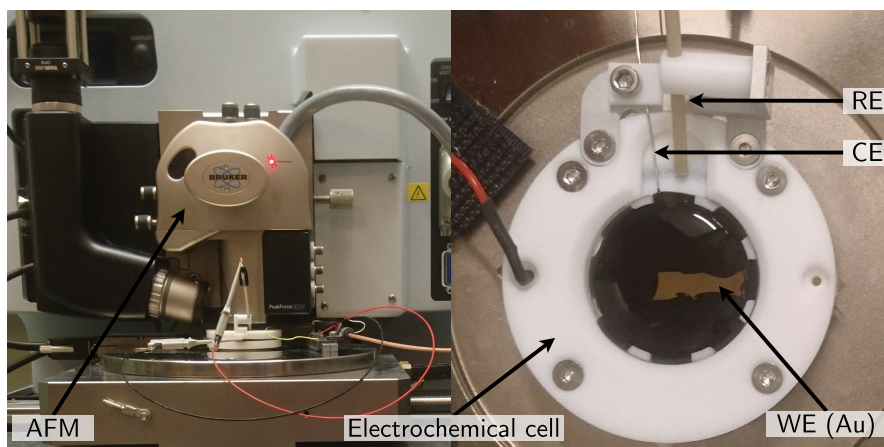
Figure 4 – Photographs of the experimental setup with the electrochemical cell placed on the AFM stage on the left, and a close-up of the electrochemical cell on the right. The reference electrode (RE), the working electrode (WE) and the counter electrode (CE) are indicated. The Au-covered Si-substrate used in this photograph has a layer of insulating wax on top of it.

3.1 Electrochemical cell

Electrochemical cells are devices that allow for conducting experiments in a controlled electrochemical environment. While it is a broad term, covering most systems consisting of electrodes immersed in a bath with an electrolyte solution, a specific type is of interest for this research. Used here, is an electrochemical cell with three electrodes, that are connected to the potentiostat in a circuit that is schematically shown in figure 5.
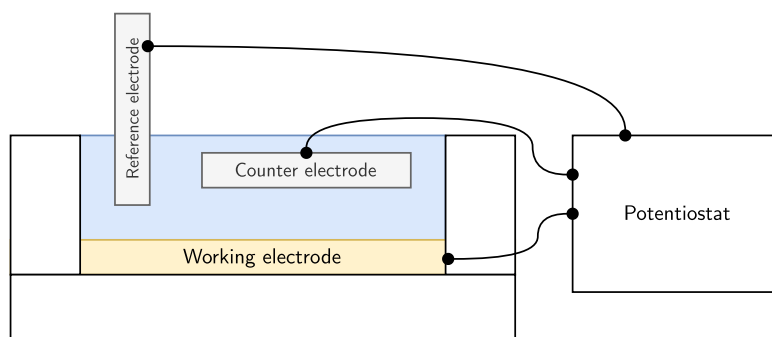
Figure 5 – Schematic representation of the circuit of the electrochemical cell, with a three-electrode system, these being the reference electrode (RE), the working electrode (WE) and the counter electrode (CE).

These electrodes are the reference electrode (RE), the working electrode (WE), and the counter electrode (CE). In the electrochemical cell, a potential difference is applied

between that CE and the WE, creating an electric field inside the liquid. As a result of the applied potential, reduction or oxidation half-reactions can take place at the WE and the CE, which serve as either the cathode or the anode. The surface area of the CE must be of comparable magnitude to that of the WE, to ensure that the reaction at the WE can occur unimpeded [23]. Moreover, no current is meant to flow through the RE, enabling the RE to set the potential of the other electrodes [46]. In the experiments of this thesis, the AFM tip was not used as an electrode. Thus, the tip was at a floating potential.

Completing the circuit, and setting and measuring the electrochemical parameters, is the task of the potentiostat. The potentiostat is connected to a special electrochemical stage of the AFM, which allows for easy connections within the available space in the AFM. It supports the automatic performing of electrochemical experiments such as cyclic voltammetry, open-circuit-voltage measurements, and chronoamperometry as well as more advanced experiments. The potentiostat works to achieve the requested potential by measuring the potential between the WE and the RE and using the CE to deliver the desired potential.

Specifically for the experiments of this thesis, we used an in-house fabricated electro-chemical cell (visible in figure 4). All parts of the cell that come into contact with the liquid, such as the top plate, are made of PTFE (Teflon), which is chemically stable, and easy to keep clean due to its hydrophobicity. Some screws and the bottom plate are made of aluminium. The bath has a diameter of about $26\,\text{mm}$, giving it an approximate volume of $2.6\,\text{cm}^3$ with a height of $5\,\text{mm}$.

In the cell, a sample can be mounted as a working electrode. The sample is placed in between the two halves of the electrochemical cell body that are held together by screws. An O-ring between the working electrode and the upper part of the cell body keeps the bath watertight to prevent leakage and short-circuiting. In the bottom part of the cell, magnets are embedded that connect to the AFM stage to hold the cell at a constant location and orientation.

At the topside, on the inside of the hollow bath of the upper part of the cell body, the CE can be mounted in small ridges at the edge of the bath. The CE that was used was a custom platinum electrode in the shape of a loop. It has this shape to maximise its surface area within the geometry of the cell, which is – as earlier mentioned – important, to generate a uniform electric field and to allow for the head of the AFM to enter the cell. Finally, a reference electrode can be mounted at the side of the cell. It is inserted into the liquid in a side-bath, to prevent it from touching the AFM head.

The RE that was used is a leakless silver chloride (Ag/AgCl[9]) electrode from Mengel Engineering. Before each experiment, it is calibrated against a full-size Ag/AgCl RE of the brand Radiometer Analytical, model XR300 which has a porous pin junction. This calibration is performed in a solution of $1\,\text{M Na}_2\text{SO}_4$. The measured potential of the REs is monitored by logging it with a potentiostat of the brand Biologic (model SP-300) that is controlled by EC-lab software v11.3. This enables the measured potentials in the experiments to be converted from a potential versus the RE to a potential versus Ag/AgCl using the following simple equation:

$$V_{\text{measured vs. Ag/AgCl}} = V_{\text{measured vs. RE}} + V_{\text{RE vs. Ag/AgCl}}. \tag{17}$$

Here, $V_{\text{RE vs. Ag/AgCl}}$ is obtained by taking the average value of an open circuit potential (OCP)-measurement that runs for 2 minutes. Typically, the deviation in potential during such a measurement is just $2\,\text{mV}$.
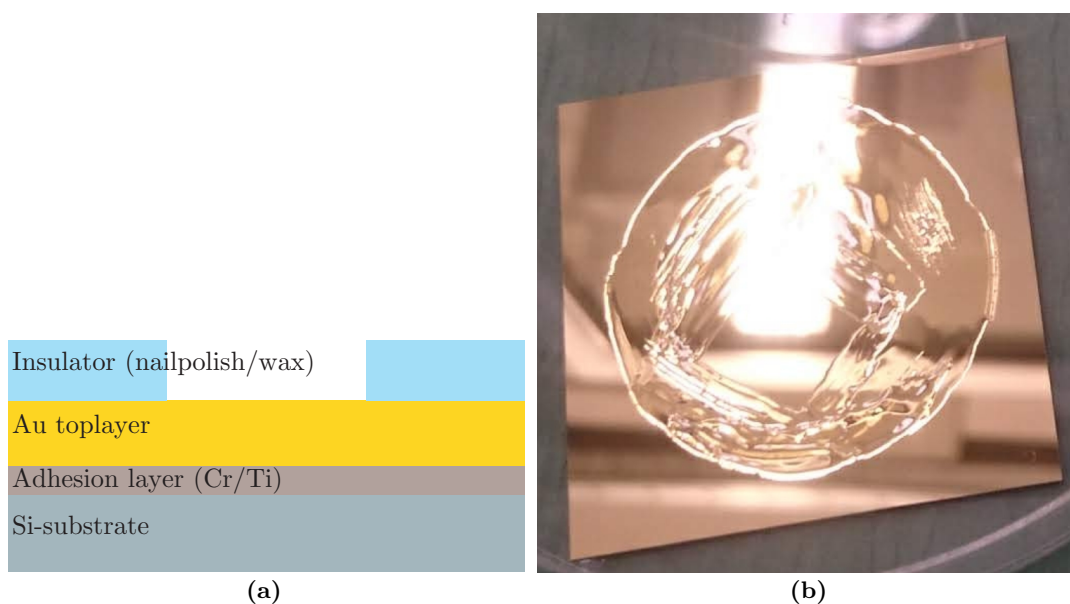
---

[9]For reference, $V_{\text{Ag/AgCl}} = 0.197\,\text{V}$ vs. NHE [5].

During the research period, two electrochemical cell designs have been used. The second design improved on the first design by adding a side-bath where the RE can be inserted into the liquid, whereas in the first design the RE had to be inserted into the main bath of the cell. Because the opening of the cell is of comparable size to the AFM-head, in the old design it was tedious to fill the bath to the correct volume without overflowing and to prevent the AFM-head from touching the RE.

3.2   Substrate fabrication

Like the electrochemical cell, the gold working electrodes that were used in this research were custom-made. They are p-type silicon wafer substrates cut into a square shape, with a 100 nm Au-layer on top of it. Figure 6a shows a schematic sideways cut of how the substrate is structured. In between the gold and the silicon, there is an adhesion layer that holds the two materials together, which is made of 5 nm Cr or Ti.

In order to reduce the conducting surface area of the WE, an insulating layer of for example nail polish is placed on top of the gold layer, leaving open a square uncovered gold window. This window is where the AFM data is collected and can be seen in figure 6b, where it can be seen that it is made in a shape that allows for an easy calculation of this surface area[10]. Aimed is for a surface area of approximately $1 \, \text{cm}^2$, which is of comparable magnitude to the surface area of the CE, as can be verified by computing $A_{\text{CE}} = \pi r_{\text{wire}}^2 l_{\text{wire}} = \pi r_{\text{wire}}^2 \cdot \pi d_{\text{loop}}$, where the CE is assumed to be a cylinder of radius r with a height l_{wire}. With an r_{wire} of 0.25 mm and a d_{loop} of 26 mm, a value of $1.6 \, \text{cm}^2$ is found.

| Insulator (nailpolish/wax) |
| Au toplayer |
| Adhesion layer (Cr/Ti) |
| Si-substrate |

(a)   **(b)**

Figure 6 – (a) Schematic side view of a sample, the thicknesses are not to scale. (b) Photograph of a sample, a gold-covered silica substrate with a nailpolish insulation layer.

Fabrication of the samples is done by following this procedure:

1. In the cleanroom, on the silicon wafer, an adhesion layer of 5 nm Cr or Ti is coated on the wafer. This is done either by sputtering, with a Leica EM ACE600 Double sputter coater, or by evaporation, with an Electron Beam Physical Vapor Deposition machine (E-Beam PVD system Polyteknik).

2. In the cleanroom, on top of the adhesion layer, a 100 nm Au-layer is either sputtered or evaporated.

---

[10] Knowing the surface area of the working electrode is necessary for converting the absolute current values collected by the potentiostat to be converted into more relevant current density values.

3. The substrate is cleaved into two square pieces of $4\,\text{cm}\times4\,\text{cm}$, that fit into the electrochemical cell. Afterwards, the substrate is cleaned of cleaving shards by rinsing it with milliQ-water and drying it using a N_2-spray.

4. The area within the O-ring is covered with insulating wax or nail polish, except for a square in the middle. The nail polish is simply applied using its brush, the wax is heated slightly before it is also applied directly to the sample (the wax is crayon-shaped).

5. The insulating layer is left to dry overnight in a fume-hood.

6. The sample is cleaned by rinsing it with milliQ-water, drying it using a N_2-spray, and placing it in a plasma ozone cleaner for 15 minutes.

Before using it in an experiment, a reference topography image of the substrate is made using the AFM. An example of such an image is visible in figure 7. The next part will explain more about how an AFM works.
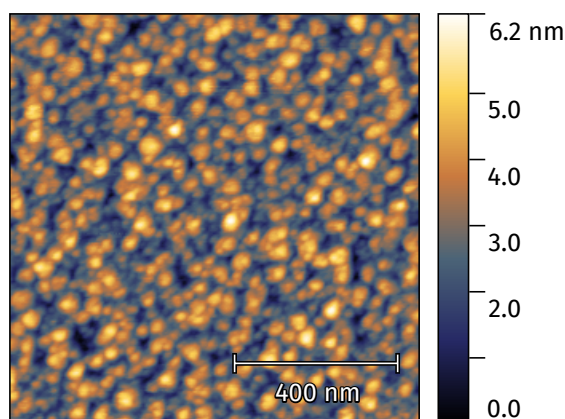

Figure 7 – Reference $1\,\mu\text{m}\times1\,\mu\text{m}$ topography AFM-image of the gold surface of the sample SputterGold. The scale bar is $400\,\text{nm}$.

3.3   Atomic force microscopy

The main tool used in this research is the atomic force microscope (AFM), a type of scanning probe microscope (SPM) that images an object not using radiation (electron or light) but using mechanical interaction: it 'sees' by 'touching'. For this, it uses a small tip ($\sim5\,\mu\text{m}$ tall, $\sim20\,\text{nm}$ in radius [34]), like a record player needle, that is attached to the end of a slightly less small cantilever ($\sim70\,\mu\text{m}$ long) to scan along the surface of interest. Specifically, we used a Bruker Dimension icon AFM.

In figure 8, a drawing of an AFM is displayed. Using piezo controllers, the x-, y- and z-position of the cantilever with respect to the stage can be controlled accurately, allowing the researcher to move the tip towards the surface at a specified position. While the tip approaches the surface, forces between the surface and the tip cause the cantilever to bend. Meanwhile, a laser shines on the reflective back of the cantilever. The reflected beam is detected by a photo-diode, which is divided into four quarters. By monitoring the strength of the signals in the quarters, the system can translate a ridge on the surface, into a bending of the cantilever, into a deflection of the laser beam and a signal.

Different types of tips can be used, and the tip is placed into a tip holder which goes into the scanning head of the AFM. In order to reduce the effect of external vibrations on the measurements, an active vibration control system is used. Moreover, the AFM can be operated in different modes, most of which scan the xy-plane periodically while controlling the z_{height} in some way that differs across modes. First developed was the
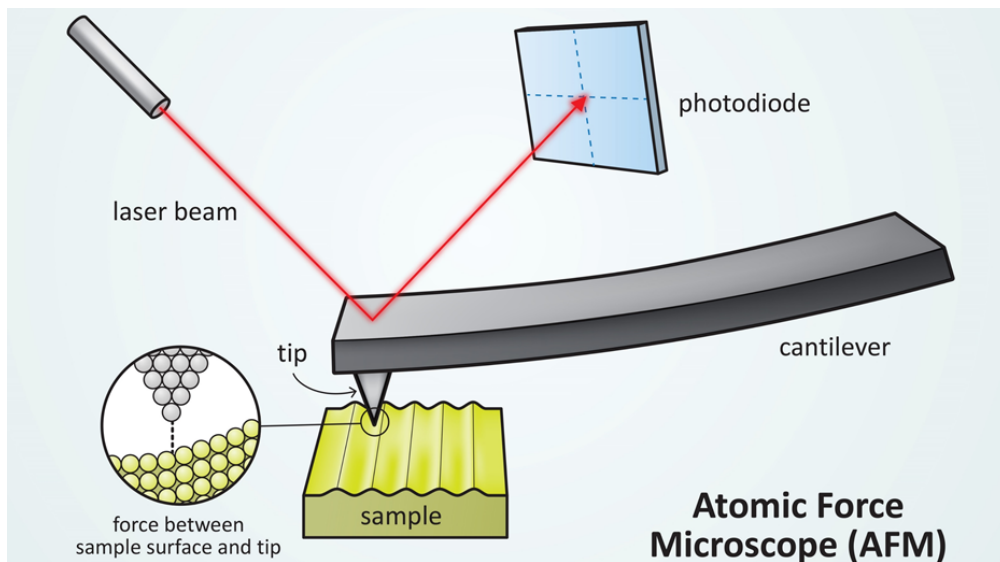
Figure 8 – Schematic representation of the working principle of an AFM: the cantilever scans a surface, with the laser beam reflecting from its back to the photo-diode, which measures the cantilever deflection [47].

contact mode, where the tip is dragged over the surface and either the force or the distance to the surface is kept constant while the other of the two quantities are measured. It is adequate for mapping the topography. However, this 'scraping'-like method can damage the surface.

Another mode is called the tapping mode, where the cantilever is driven to its resonant frequency and the tip thus oscillates over the surface, while the deflection of the cantilever allows for mapping the surface. In our experiments, we used the peak force tapping (PFT) mode, specifically an implementation by Bruker [15]. A combination of pN-sensitivity and real-time deflection monitoring allows the AFM to lower the cantilever until a certain maximum force is observed, the peak force setpoint (PFS). This method has the advantage that it is less destructive to the surface, making it suitable for biological samples.

As the AFM tip oscillates over the substrate, the deflection of the cantilever is measured. Figure 9 shows what happens. As the tip approaches the surface, once it gets close
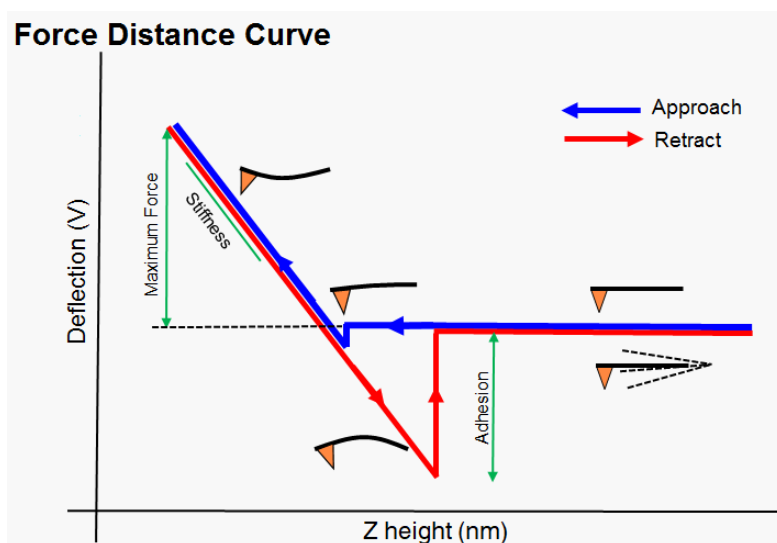
Figure 9 – Sketch (cantilever) deflection–z-height force curve, consisting of the approach (blue) and retract (red) curve. The shape of the cantilever is shown at different heights. The adhesion, maximum (peak) force and stiffness (elasticity) are indicated [47].

enough for the surface to exert a force on the tip, the cantilever will deflect upwards, which is observed as a rising positive deflection. Because the cantilever is a spring with a measurable spring constant, this deflection can be converted to the force exerted on the tip using Hooke's law, $F = kx$, where F is the force, k is the spring constant and x is the extension of the spring (in this case the cantilever).

Once this force reaches the PFS the tip is retracted, causing the cantilever to bend back to zero deflection. After the main peak, an attractive peak occurs. This phenomenon, adhesion, is a result of van der Waals forces. The shape of the force curves provides information about the properties of the studied material, and extracting these properties is of interest to us.

4   Experimental methods

To paint a full picture of the experiments, in this part the methods used to work with the set-up are described. First, the electrochemical techniques that were conducted in the electrochemical cell are explained. Secondly, the main method with which the AFM was used is explained. All experiments are based on the principle of creating certain electrochemical conditions in the cell and then measuring AFM-force curves simultaneously.

4.1   Electrochemical methods

The CH-instruments potentiostat that was used supports many experimental techniques that apply to the three-electrode system in the electrochemical cell. In the following, the techniques that were used are explained.

4.1.1   Open circuit potential

Before each experiment, an open circuit potential (OCP) measurement was performed. In an OCP, the potentiostat measures the potential between the WE and the RE over time, which has two use cases. Firstly, it is used for calibrating the RE (see equation (17)). Secondly, the OCP–t graph shows if the system is stable or not. If the OCP varies more than around $10\,\mathrm{mV}$, there might be a source of noise and if the OCP contains a (linear) trend, EC-reactions might be ongoing. Both indicate an unstable system.

4.1.2   Cyclic voltammetry

A key technique in electrochemistry is cyclic voltammetry (CV): an experiment where the potential (U) is swept back and forth across a certain range, while the current (I) is recorded. For a bare electrical circuit, an Ohmic response is expected, with the curve forming a straight line with slope $R = U/I$. In an electrochemical experiment in absence of charge carriers, an almost horizontal line is observed: the high resistance allows for little current to flow. However, in a solution with free ions, current can flow and on top of the normal current, redox-reactions can occur in the electrochemical cell. These cause peaks in the CV-curve at specific locations, that can be used to map the so to say 'potential-landscape' of the system and identify certain reactions taking place.

In figure 10a an example of how a CV-curve looks theoretically is shown. The characteristic shape of this curve causes it to be sometimes called the 'duck curve' of electrochemistry. Following the international (IUPAC) convention, the peak at the top is associated with an oxidation reaction and that at the bottom with a reduction reaction [46].

(a)   (b)
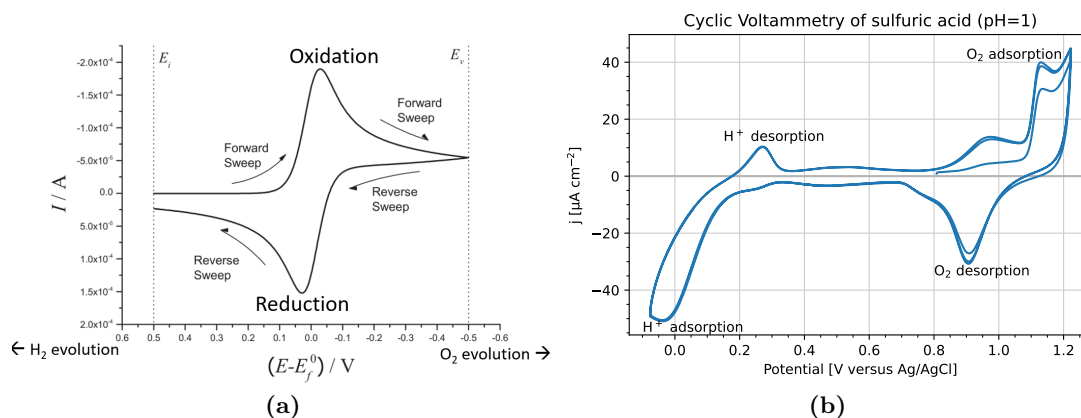
Figure 10 – (a) Theoretical CV-curve. (b) Experimental CV curve of a gold electrode in H_2SO_4 (NailGel sample) with annotated peaks, recorded at a scan rate of $50\,\mathrm{mV/s}$.

17

Figure 10b shows a CV-curve that was collected during the experiments. It is collected in H_2SO_4 with a gold working electrode, at a scan rate of $50\,\text{mV/s}$. The peaks related to H^+ and O_2 adsorption and desorption on the gold surface are indicated. They occur at locations similar to those found in literature – as § 2.4 explains in more detail. In the CV curve, a negative peak is visible at around $0.9\,\text{V}$. This peak has previously been attributed to desorption of oxygen on the gold surface [43, 45]. The three smaller upwards peaks in between 1.0 and $1.3\,\text{V}$ correspond to the adsorption of oxygen. Moreover, the downwards peak at around $0.1\,\text{V}$ can be attributed to hydrogen adsorption on the surface, and the upwards peak at around $0.2\,\text{V}$ to its desorption.

At potentials even lower than $0\,\text{V}$, hydrogen will start to evolve, and at potentials larger than $1.2\,\text{V}$ oxygen will start to evolve.

4.1.3   Chronoamperometry

Another simply electrochemical technique that was used it chronoamperometry (CA or I–t). Here, a specified voltage is applied for a certain amount of time, and at short intervals the current is measured. It gives a clear look at the dynamics of an electrochemical reaction because the current that is flowing is related to those dynamics. For initial experiments, this technique was used to apply a certain voltage for a certain amount of time, and then to move to another voltage. Despite this being a robust measurement method, for later experiments more advanced techniques were used, for two reasons. Firstly, with consecutive CA-measurements, one does not know the potential of the system in between measurements. Secondly, using multiple consecutive CA measurements is less computer-controlled and thus more laborious and less consistent.

4.1.4   Staircase voltammetry

In order to improve on the previous mentioned issues with multiple CA-measurements, several experiments were performed using staircase voltammetry (SCV). This is a technique were over time, the potential is increased from V_0 to V_f with step dV, as can be seen in figure 11a.
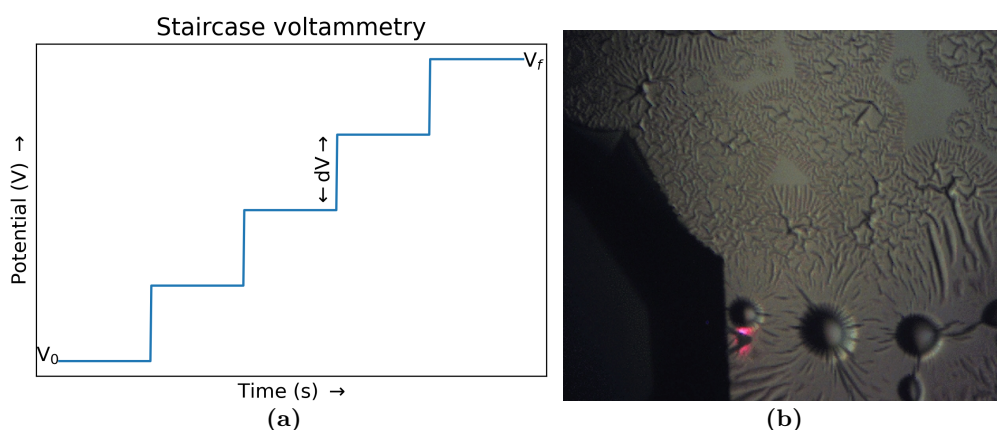

Figure 11 – (a) Sketch graph of a staircase voltammetry (SCV) experiment, where the potential moves from V_0 to V_f in steps of dV. (b) Optical microscope photograph of the gold layer peeling off due to bubble-formation. The cantilever and laser spot are visible.

A problem with this technique that was initially overlooked, is that due to its nature, the system is kept at potentials where the current is also higher for prolonged times. At high potentials, this led to oxygen accumulating in and underneath the gold-layer of the substrate, which lead to bubbles that caused the gold layer to peel off. An optical microscope photograph of the process can be seen in figure 11b. Another negative of this

technique is that in the used potentiostat, this technique only records one current data point for each potential.

4.1.5   Normal pulse voltammetry

To avoid the problems of the previously mentioned methods, we used normal pulse voltammetry (NPV). As figure 12 shows, in such an experiment the potentiostat applies a base potential ('Init E' in the figure) alternated with a pulse potential. The potential of the pulse is increased by steps of 'Incr E' from 'Start E' (also called V_{base}) to the pulse height V_{pulse} until the pulse height reaches 'Final E'.
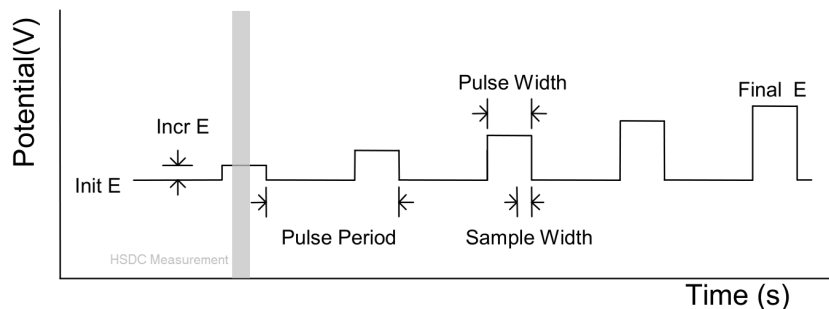
Figure 12 – Sketch graph of a normal pulse voltammetry (NPV) experiment, where the potential goes from V_{base} to a pulse of height $V_{pulse} = n \cdot V_{incr}$ for increasing or decreasing n until the potential reaches V_f [48].

In the experiments of this thesis, the parameters for the normal pulse voltammetry were determined as follows. First, a CV-curve of the system is determined. Then, V_{base} is chosen as a value which lies in the flat part of the CV, where current I is low. The start and the final potential are chosen to either include or exclude certain peaks in the CV. This depends on which electrochemical processes are investigated. We chose to include the redox peak-pairs, but to exclude the oxygen and hydrogen evolution parts (at high and low potentials, respectively) – because in these parts I becomes high and bubbles could form, which disturb the AFM-measurement.

Furthermore, the pulse period was set to 40 seconds, and the pulse width to 10 seconds. So, the time in between pulses was 30 seconds, during which we saved the previous measurement in the AFM-software and prepared for the next one. During the 10 seconds of a pulse, after a delay of ~2 seconds[11], an AFM-measurement with a duration of 2 seconds was performed.

4.2   AFM High-speed data capture (HSDC)

The AFM part of the measurement is conducted as follows. While the potentiostat applies a certain potential, the AFM performs a so-called high-speed data capture (HSDC) measurement. During such a measurement, the AFM scans across the surface in PFT mode and saves each force curve. Deflection and height data can be recorded at a frequency of 2 kHz. The resulting data, which looks like figure 13, is a file containing many force curves. In the case of the experiments of this thesis, mostly, measurements were made for a duration of 2 seconds, resulting in a file with 4000 force curves. These force curves can be used to extract information about the surface that was scanned such as nanomechanical properties and its topography. Depending on whether one is interested in spatial variations, one can choose how the AFM scans the surface: either it can stay at a single spot, or it can scan along a single (the x) axis, or it can scan across the xy-plane.

---

[11]This delay was chosen to ensure that the system would be equilibrated to the new potential. After 2 seconds most of the current has already flowed.
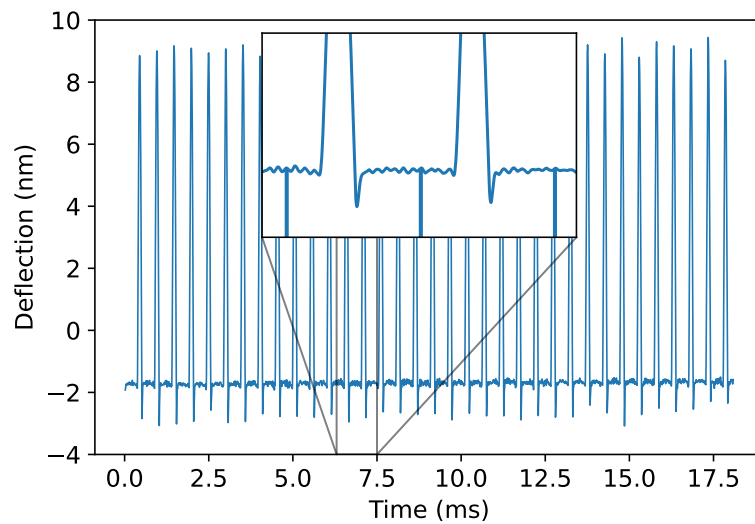
Figure 13 – Deflection–time plot of the first 17 ms of the full 2 s of an HSDC measurement, showing many force curves. The zoomed inset shows how in between force curves, a dummy data point is added to make it possible to separate the individual curves, as described in § 5.4.

5 Development of a flexible AFM data analysis method

In order to obtain useful information from the AFM measurements, it is interesting to record many force curves using the HSDC-mode. The large amount of force curves then allows for averaging which reduces the noise content of the force curves. These cleaner force curves ameliorate further analysis. Moreover, the large number of force curves that is collected can also be used to map nano-mechanical properties.

Before we can analyse the force curves, we need to perform some data treatment steps. This is because the Bruker AFM stores its data in a proprietary file format which can be opened in Bruker's NanoScope Analysis software (version 1.8). Though decent, this software does not allow for all the desired flexibility of analysis, and bulk exporting data is not supported. Therefore, we developed a data analysis toolkit in Python[12] that can open an AFM data file and extract useful information out of it. In the following part, I will lay out how this works.

5.1 Reading out HSDC files

The data from an AFM measurement is stored in a `.hsdc` file. This is a file that starts with a text-based header of around one thousand lines containing all settings and parameters of the AFM at the time of the measurement, followed by the actual data, which is binary-based. All information that is relevant for the analysis can be extracted from the file header using the Python file `hsdc_parameter_reader.py`, which can be seen in appendix A.6. Such parameters include data-related parameters like the location of the data in the file and the length of the data, as well as equipment-related parameters like the amplitude and frequency of the tapping mode of the AFM. The file extracts the parameters, stores them in a dictionary, and converts them to suitable units. Then, the data has to be extracted from the binary part of the file. This part has space for two data channels, such as `deflection`, `height` and `height sensor`. The difference between height sensor and height is that the former is the raw extension of the z-piezo, which includes the sine-wave signal from the tapping mode, and the latter is the measured height of the sample with the tapping signal removed by the AFM-software. In our code, height sensor can be converted to height data.

5.2 From deflection–time to deflection–height

The raw data that is contained in an HSDC file can be read out using the following code:

```
1    f.seek(DataOffset_def)
2    np.frombuffer(f.read(DataLength_def), np.int16)[::2].astype(float) /
         65536.0
```

Here, first, the header of the file is skipped until the part containing the data (`Data Offset`). Then, the data is read for the whole length of the data (`DataLength`). The even data points are discarded because only the odd data points contain the actual data. It is unknown why the even data points contain no data. The value is divided by $2^{16} = 65536$, because it is stored in 16-bit format.

The obtained data then needs to be multiplied by the scales: the hard and the soft scale. The physical meanings of these scales depend on the measured quantity. In this case, for the deflection, the hard scale converts the raw data to volts, and the soft scale converts the data in volts to nanometres. On the left in figure 14, one deflection–time force curve is shown.

With the deflection data extracted, the next step is to pair the data points with a suitable x-axis: time. Time data is not stored in the HSDC file but can be regenerated using

---

[12]Specifically `Python 3.9` in combination with `numpy 1.21.2`, `scipy 1.8.0` and `pandas 1.4.0`.

the `hsdc_duration` that is stored in the header of the HSDC file. The time during the measurement is stored in an array of `DataLength` equally spaced data points between zero and `hsdc_duration`.

To arrive at a force curve, the next component that is required is the Z height, briefly z_{height} or z, which can be generated similarly. It is also possible to store the measured height in the *Height Sensor* channel of an HSDC file, but the difference between this measured and the generated data is negligible. To calculate the height, the following formula can be used:

$$z(t) = A_{\text{PF}} \cdot \cos(2\pi f_{\text{PF}} t - \phi) + A_{\text{PF}}, \tag{18}$$

where z is the height as a function of time, A_{PF} is the peak force amplitude, f_{PF} is the peak force frequency, and ϕ is the sync distance. These parameters come from the HSDC file header. Equation (18) produces a sine wave tapping curve, as expected, which figure 14 shows for one force curve. By definition, $z = 0$ at $2A_{\text{PF}}$ above the point where the peak force is measured, and increases as the z-piezo extends downwards. However, the absolute values of z are arbitrary.
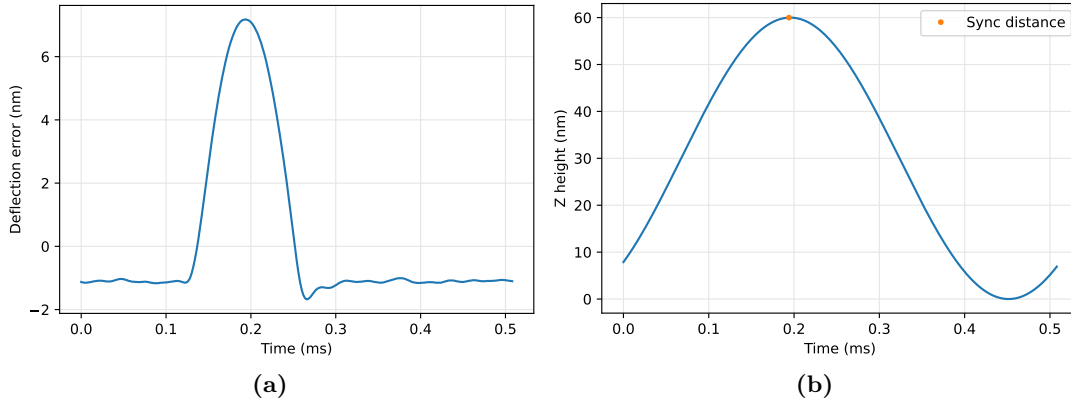
Figure 14 – Graphs showing two channels of a force curve: (a) deflection–time, (b) z–time (with the location of the sync distance indicated in orange).

For further analysis, it is useful to convert these deflection–time curves to deflection–height curves, by combining the y axes of the two graphs in figure 14, resulting in figure 15. Here, the linear response at higher z_{height} is clearly visible, and the curve is split into a trace and a retrace-curve, using the earlier mentioned sync distance to find the point of maximum z_{height}.
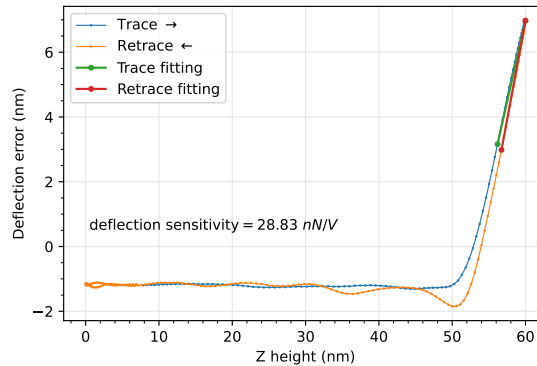
Figure 15 – Deflection–height force curve that shows deflection sensitivity calibration on the final 20 data points of the approach (green) and retrace (red), so `dif = 20`.

One important parameter in the analysis is the deflection error sensitivity (DES). This value is calculated during the calibration of the AFM at the start of a measurement by acquiring one deflection-error versus z_{height} force curve using the 'single ramp' function.

By placing markers around a part of the force curve's linear section, the NanoScope software combines the information the AFM has about the z_{height}-extension of the Z-piezo and the voltages measured by the photodiode into the DES in nm/V. This value is stored as the High Speed Data Soft Scale for the deflection-channel in the HSDC-file. It is calculated at the start of each measurement cycle.

To improve the accuracy of the analysis, the DES can be recalculated for every individual force curve. This recalibrating is done by dividing the deflection data by the slope of the linear part of the deflection-height curve, as can be seen in the following code snippet:

```
1   dif = 20
2   ratio_ext = (sub_def[sync_d] - sub_def[sync_d - dif]) / (sub_z_height[
        sync_d] - sub_z_height[sync_d - dif])
3   ratio_ret = (sub_def[sync_d + dif] - sub_def[sync_d]) / (sub_z_height[
        sync_d + dif] - sub_z_height[sync_d])
4   sub_def /= ratio_ret
```

Here, `dif` sets the amount of data points from the maximum that is used for calibration, `ratio_ext` uses the approach curve for the calibration, and `ratio_ret` the retract-curve. Using this recalibration is necessary for a robust result in the step described in the next section.

5.3   Force–separation curves

While the AFM provides the data with z as the x-axis, this experimental relevant parameter is less suitable for physical interpretation of the force curves. More suitable for this is the separation between the sample and the AFM tip. Since in the experiments the sample is a hard surface, its calculation is straightforward. As can be seen in figure 16, the separation can be described by the following formula:

$$\text{separation}(t) = z(t) - \text{deflection}(t), \tag{19}$$

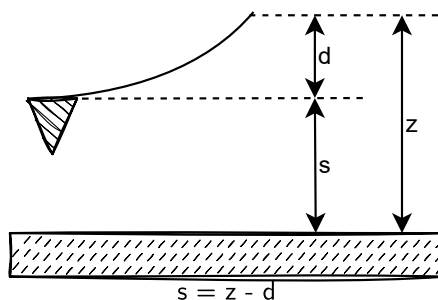where z is the distance between the cantilever and the surface.

Figure 16 – Visual aid for understanding equation (19).

This z is not the same as the measured quantity Z height, since that is the distance by which the Z piezo has extended downwards, roughly the Z distance between the part of the AFM body holding the scanner head and the cantilever. In order to find the correct values for the separation, the separation values are subtracted from their maximum value for that force curve, as can be seen in the following code:

```
1   sub_sep = sub_z_height - sub_def
2   sub_sep = sub_sep.max() - sub_sep
```

In other words, the point of zero separation is defined here by this maximum value in the contact part of the force curve.

The final step in obtaining a physically interesting force curve is converting the deflection error values to force values. This can be done because the cantilever is a spring with a

well measurable spring constant k. In the NanoScope software, using the ThermalTune function the spring constant is determined by driving the cantilever away from the sample. By fitting the resonant frequency to a simple harmonic oscillator model, the spring constant is calculated and stored in the HSDC file as the `@Sens. ForceDeflSens` in nN/V (more details of the procedure are provided in [15]). In our analysis code, the spring constant is calculated as follows:

```
spring_k = force_defl_sens / soft_scale_def   # N/m
```

Using this calculation of the spring constant yields a value with more significant figures than can be found in NanoScope Analysis.

With the spring constant determined, the force data simply follows from Hooke's Law,

$$F = \text{deflection} \cdot k. \tag{20}$$

The result of the analysis is that from the raw data, a force–separation curve has been extracted and reconstructed. As can be seen in figure 17, the found force curve is ready to be compared to theoretical models of tip–sample forces. However, for contact mechanics analysis, it would be useful to convert the force into pressure, by calculating the contact area using the tip radius. Figure 18 shows a summary of the discussed parameters and

(a)   **(b)**
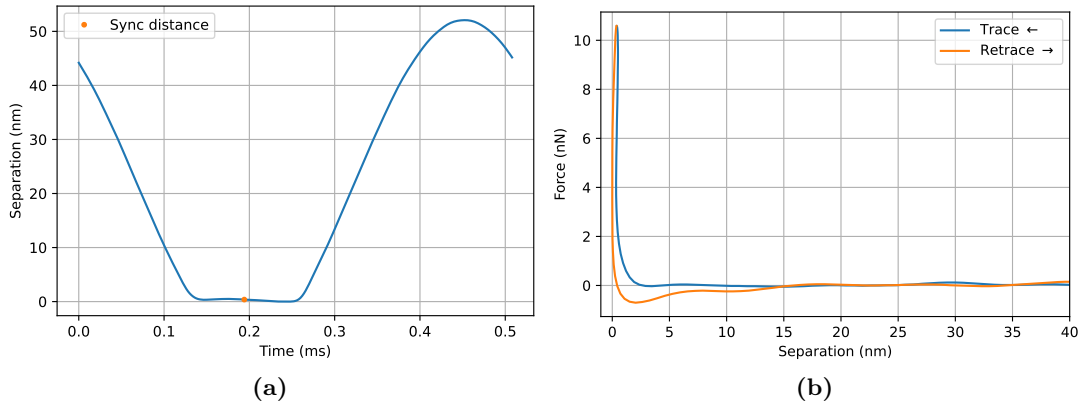
Figure 17 – Graphs showing two channels of a force curve: (a) separation–time, with the sync distance indicated in orange, (b) force–separation.

their relations.
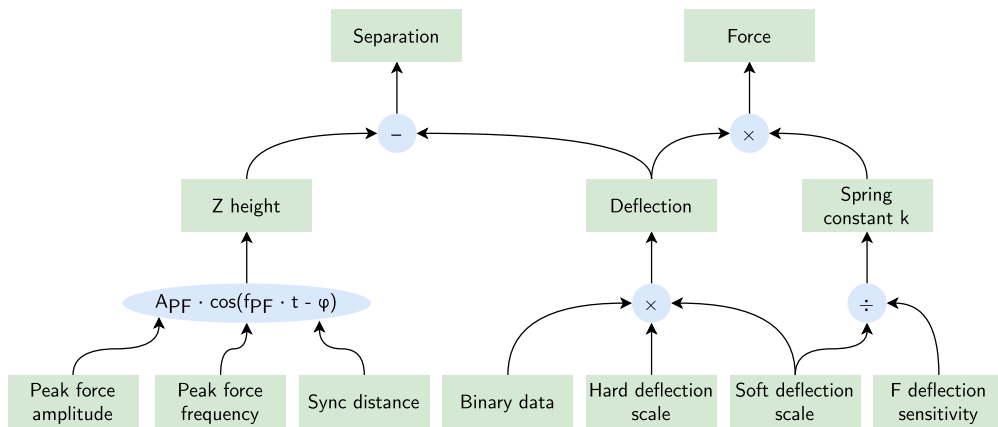
Figure 18 – Graphical summary of the steps that are taken to distill the useful quantities force and separation from the raw data.

5.4 Peak separation

Within the HSDC file, all individual force curves of a measurement are stored together in one file. However, it is possible to separate the force curves from each other because an extra data point with an unphysical value is added at the beginning of each force curve, the curve separator (this can be seen in figure 13). Thus, the peaks can be separated using the following code, for finding force curve i:

```
1   curve_separator = -0.5
2   peaks = np.nonzero(force_dat == curve_separator)[0]
3   sub_force = force_dat[peaks[i] + 1:peaks[i + 1]]
```

making use of NumPy's `np.nonzero` function.

5.5 Peak detection

For numerical analysis, it is useful to determine the height of the peaks of a force curve. To do this, a peak detecting algorithm is used that is available in the package `scipy.signal` of the SciPy Python module, called `find_peaks` [49]. In the following code it can be seen how this algorithm is used to find local maxima.

```
1    from scipy.signal import find_peaks
2    prominence_threshold = sub_force.max() - sub_force.mean()
3    f_peaks, f_peak_props = find_peaks(
4      sub_force,
5      prominence=prominence_threshold,
6      distance=points_per_window - 1,
7      width=0)
8    f_minmax, f_minmax_props = find_peaks(
9    np.append(sub_force.min() - 1, sub_force),
10   prominence=prominence_threshold,
11   distance=points_per_window - 1,
12   width=0)
13   if len(f_peaks) == 0:
14     # discard this force curve
15   peakforce = f_peak_props["prominences"]
16   minmax = f_minmax_props["prominences"]
17   adhesion = minmax - peakforce
```

Here, `f_peaks` means the force peaks found in the `sub_force` array that should contain one force curve of the HSDC dataset. Prominence means the minimum height of a peak that the algorithm will recognise in the input. In the output it, means the found height of a peak. The peak detecting algorithm is applied twice. Firstly, in lines 3 to 7, to find the height of the main positive peak above the baseline of the force curve. Secondly, in lines 8 to 12, to find the 'minmax' distance between the height of the main positive peak, and the negative dip. In line 9 a value is added to the array that is trivially, but significantly lower than the minimum of the array. Due to this new lowest value, the algorithm triggers its prominence measurement from the top to the bottom of the force curve, instead of from the top to the baseline. These two heights can be used for finding the adhesion, which is described in the following part.

5.6 Nanomechanical properties

With the information about the peaks of a force curve, the nanomechanical properties of the system can be calculated. These nanomechanical properties are local mechanical material properties at the location of the AFM tip, such as Young's modulus, adhesion, dissipation, deformation and elasticity. For a force curve, these properties can be calculated. Since the data treatment method enables numerical analysis of force curves, each nanomechanical property can be calculated. In this work, this is done for the adhesion and the elasticity.

The adhesion is the depth of the lowest point of the force curve with respect to the baseline. It is calculated in line 17 of the code in the previous section. Physically, it describes how much the AFM tip sticks to the surface during the retracting phase of the force curve. The elasticity can be calculated as the derivative of a force versus z_{height} curve, i.e. $E = \frac{\mathrm{d}F}{\mathrm{d}z}$ in units of N/m. It gives information about how deformable the surface–cantilever system is at a certain z_{height}. This Python code calculates the elasticity:

```
elas_approach = np.gradient(force[:sync_d], z_height[:sync_d])
elas_retract = np.gradient(force[sync_d:], z_height[sync_d:])
```

for the approach part and the retrace part respectively.

5.7   Averaging

While the obtained force curves are quite robust, temporal noise and spatial variations introduce some uncertainty in its analysis. To improve the accuracy, and allow for a better comparison of numerical values, the force curves can be averaged. As mentioned, the HSDC method produces many force curves. For looking at the profile of the force curve, both the force and the separation can be averaged across all force curves of a dataset to obtain an average force curve. This average force curve typically has a cleaner appearance. For numerical comparisons, the nanomechanical properties of all force curves of a dataset can be averaged. This averaging makes it easier to compare the AFM data between different electrochemical situations. However, it is also interesting to use plotting forms that allow for visualising the temporal and spatial distributions of force curves within a scanning spot, line, or square.

5.8   Analysing the EC-data

Electrochemical data of the CH Instruments potentiostat is acquired using its included software that is called 'CHI760E Electrochemical Workstation'. For each measurement data is stored in two files: a `.bin`-file that can be opened in the CH-software, and a `.txt` plain text file that can be read with custom Python-scripts. An example of such a text file can be seen in appendix A.6. It is structured with first a header containing experimental parameters and second the data in comma-separated values. The data is read using the `skip_to` method of the file `module_file_reading.py`.

6 Comparing adhesion for different electrolytes

With the goal of exploring the system of interest of this thesis and designing an experiment, we compared the behaviour of different solutions as liquids in the electrochemical cell.

For the different solutions, the following measurement scheme was used: a constant potential between the working electrode and the counter electrode is applied, while simultaneously the AFM collects force curves in an HSDC measurement. No reference electrode was used, so the absolute potentials are arbitrary. This is manually repeated for ~10 voltages in between -2 V and 0.2 V. While this is similar to normal pulse voltammetry, the manual constant V-mode of the potentiostat was used, so in between measurements the potential is uncontrolled. Due to the exploratory nature of these measurements, more rigorous electrochemical techniques were still unfamiliar to me, and less relevant.

By varying several parameters – electrolytes, pH and concentration –, we conducted such a measurement for different electrochemical conditions. Table 2 shows the details of the solutions. We conducted measurements without solvates in the cell (plain milliQ water), and with the solvates sulfuric acid (H_2SO_4), salt (NaCl) and copper sulfate ($CuSO_4$). Sulfuric acid was used because of the influence of sulfides on gold structure [42], and to

Series	Solvent	Solvate 1	Concentration	Solvate 2	Concentration	pH
M1	H_2O	-	-	-	-	7
M2	H_2O	H_2SO_4	1 mM	-	-	2
M3	H_2O	H_2SO_4	1 mM	NaCl	100 mM	2
M4	H_2O	-	-	NaCl	100 mM	7
M5-10	H_2O	$CuSO_4$	10 µM	-	-	7
M5-100	H_2O	$CuSO_4$	100 µM	-	-	7
M-1000	H_2O	$CuSO_4$	1000 µM	-	-	7

Table 2 – All the measurement series with their names and contents for the first set of experiments that compare electrolytes.

probe the effect of pH. Salt was used to probe the effect of more ions and consequently more current. Copper sulfate was used because of its application in electrochemical deposition, which is researched in the 3D-photovoltaics research group [50].

With our data analysis method, we calculated the adhesion for every AFM measurement for every solution, and figure 19 contains the results. Every data point in the plot represents the mean adhesion of all force curves of an HSDC measurement, and the uncertainty bands represent the standard deviation. As mentioned, the potentials reported on the x-axis are not versus a standard potential. Hence, it is difficult to relate the results to specific electrochemical processes.

Voltage-dependence varies among the different solutions. Sulfuric acid (orange line), is the solvent with the most striking results: at high voltages, the adhesion is the highest of all datasets (up to 3 nN); at -0.55 V, the adhesion drops to 0.5 nN with nearly no standard deviation. Salt (NaCl, red line) shows a similar pattern with a drop in adhesion at -1.15 V. These drops coincide with an increase in current.

Furthermore, the measurements for just water show little variation. There is a large difference between a low and a high concentration of copper sulfate. It should be noted that at the lowest voltages for 1000 µM $CuSO_4$, copper started to deposit on the gold surface.

Cyclic voltammetry under the conditions of the measurements shows no clear peaks in the studied -2 V–0 V region. At low voltages, the current significantly increases, which is
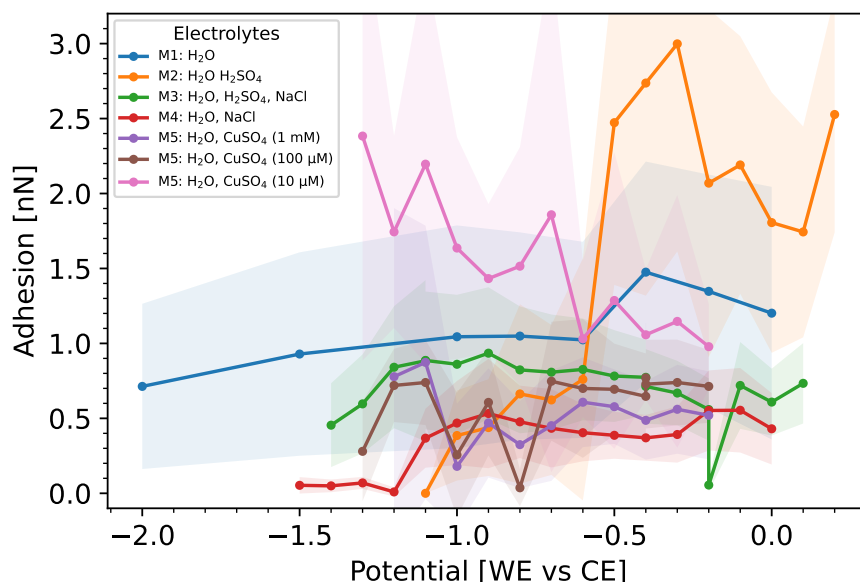
Figure 19 – Average adhesion with the standard deviation as uncertainty band (shaded) for the solutions of table 2. No reference electrode was used.

also clear in the current-data from the constant V-measurements. Despite the lack of a reference electrode, the characteristic gold oxygen desorption peak was observed around $0.8\,\text{V}$, so the reported voltages are probably only a few hundred mV versus Ag/AgCl.

Summing up, we observed clear potential dependence for the adhesion for different solutions. The largest difference in adhesion was found for the solution with sulfuric acid in water, where both high and low adhesion was observed. Moreover, the SO_4^{2-} ions that are present in such a solution form layers on the gold surface depending on the potential (see § 2.4). Therefore, we consider it interesting to continue further measurements on the aqueous sulfuric acid electrochemical system. The next chapter shows the results of these measurements.

7 Voltage-dependent force-mapping of gold

Using the electrochemical AFM-setup in combination with the data analysis method, we performed several measurements. In total, 333 HSDC-files were collected during 19 measurement series on 7 gold-samples. All measurements were performed using aqueous sulfuric acid (H_2SO_4), at a pH of ~2. Table 3 shows the experimental details of each sample.

Sample Name	Base	Adh	h (nm)	Top	h (nm)	Insulator	A (cm^2)	Machine
NailPolish Gold	Si	Cr	5.0	Au	~50	nailpolish	1.0	E-flex
NailPolish Gold 2	Si	Cr	5.0	Au	~50	nailpolish	1.0	E-flex
NailGel 1	Si	Cr	5.0	Au	~50	nail gel	1.0	E-flex
Thick Gold 1	Si	Cr	5.0	Au	100	nailpolish	1.0	E-flex
NailPolish Gold 8jan	Si	Cr	5.0	Au	~100	nailpolish	1.0	E-flex
Sputter Gold	Si	Cr	6.1	Au	101.25	nailpolish	1.0	Sputter coater
Wax Gold Ti	Si	Ti	~5	Au	~100	wax	0.8	Sputter coater

Table 3 – Gold-samples used during the experiments, showing for each sample the base layer, the adhesion layer material and thickness, the toplayer material and thickness, the insulator, the conductive surface area A and the fabrication method machine.

Samples differ in the adhesion layer, the thicknesses of these layers, the type of insulator, and the fabrication technique. The next part shows the results of the measurements on these samples.

7.1 Staircase voltammetry

Initially, measurements were performed using a staircase voltammetry (SCV) scheme described in § 4.1.4. This technique allows us to define a controlled electrochemical environment for studying the influence of potential on nanomechanical properties. Specifically, in the diluted sulfuric acid-containing electrochemical cell, three gold substrates were inserted for SCV measurements: 'NailPolish Gold 2', 'NailGel' and 'Thick Gold'.

Successfully using staircase voltammetry to study the forces at the gold layer turned out to be challenging. By inspecting cyclic voltammetry on the NailPolish Gold 2 sample, we chose to conduct a descending staircase measurement with 40 potentials from 1.5 V to -0.5 V – the V-region with reduction/oxidation peaks, but without oxygen or hydrogen evolution.

As figure 20 shows, there is a profound change in the adhesion in response to the voltage-sweep. From 1.5 V downwards, the average adhesion is 2.5 nN (high, relative to the peak force of 10 nN), but at 0.4 V the adhesion drops significantly to approximately 0.5 nN, with a low standard deviation. This coincides with the end of the reduction peak that is centred around 0.7 V in the CV, which has the shape of the oxide-desorption peak that is normally found at at least 0.8 V.

However, this measurement is not a reliable probe of the nanomechanical behaviour, because at some point during the measurement, the gold layer was peeled off the substrate by bubbles. Figure 11b shows how this looked on the optical microscope of the AFM.

The bubbles possibly formed because at the high voltages, too much oxide, or even oxygen was adsorbed into the gold layer, in combination with a high current (at 1.4 V j exceeds 100 µA/cm^2). It could be that subsequently at 0.4 V, the oxides tried to desorb, but were at such a high concentration in the gold layer, that they coalesced into oxygen bubbles, thereby destroying the gold layer.

In an attempt to overcome the bubble-issue, a measurement was conducted on the sample 'NailGel' with a narrower V-range: 0.6 V–1.3 V, and a lower pH (keeping the Pourbaix
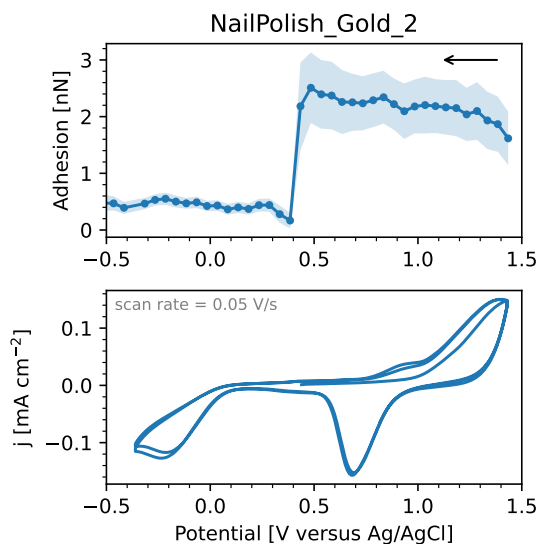
Figure 20 – Mean adhesion for the 40 hsdc measurements on the Nailpolish Gold 2 dataset, showing the standard deviation in the shaded band, including a CV on this system with a scan rate of $50\,\mathrm{mV/s}$.

diagrams of gold andS water in mind). However, during the measurement, at $1.05\,\mathrm{V}$ pits in the gold layer formed, turning into bubbles at $1.25\,\mathrm{V}$, yielding unusable results for further analysis. Another attempt was made using a substrate with a thicker gold layer ('Thick Gold', with $100\,\mathrm{nm}$ Au), which also provided no usable results due to a damaged gold layer.

In consideration of the difficulties in reaching a reliable measurement, we concluded that staircase voltammetry is an unsuitable electrochemical method for the experiments we envision. We believed that by keeping the potential at increasingly high voltages, too much charge builds up in the gold layer. Therefore, normal pulse voltammetry was used for the next measurements, of which the next part lists the results. On second thoughts, the issues with staircase voltammetry are probably not an issue with the technique *per se*, but with applying it to the high voltages where oxide formation occurs. Taking an even narrower *V*-range, focused on the double layer charging part, with a maximum of $0.9\,\mathrm{V}$, might make staircase voltammetry a useful method.
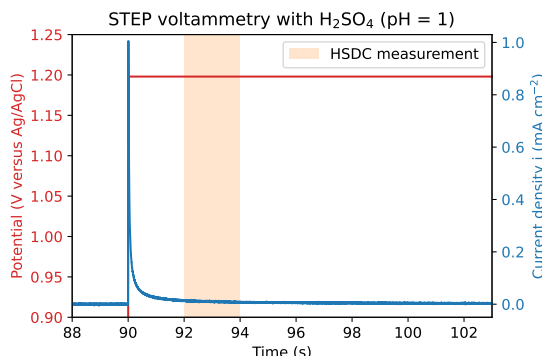
7.2   Normal pulse voltammetry

To overcome the bubble-issues, further measurements were done using normal pulse voltammetry (NPV). This method was used on the samples 'Nailpolish Gold 8jan', 'SputterGold' and 'WaxGoldTi'.

The red line in figure 21 shows the applied potential over time of one sample. It follows
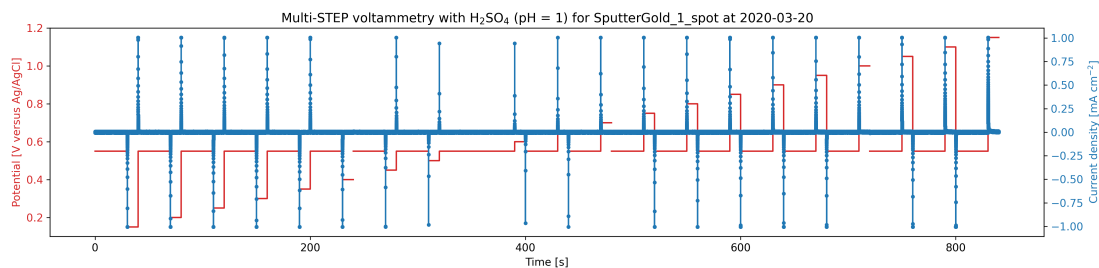
Figure 21 – Normal pulse voltammetry (realised by combining multiple step-voltammetry macros) results for SputterGold-spot dataset, showing potential–time (red) and current–time (blue).

the measurement scheme as described in § 4.1.5. In blue, the measured current follows an asymptotic decay pattern after each voltage change, which is more clear on a zoomed plot of one pulse, such as figure 22. In many cases, the current overflows – the maximum current

Figure 22 – Plot of one normal pulse voltammetry pulse, showing the potential in red, and the current in blue. The orange shaded region indicates the timing of an HSDC measurement by the AFM.

of a pulse is capped at $1 \, \mathrm{mA/cm^2}$. This is because the sensitivity of the potentiostat was too low ($1 \times 10^{-4} \, \mathrm{A/V}$). At higher voltages, more current is flowing than at lower voltages. At four places in the plot ($t = 240 \, \mathrm{s}$, $480 \, \mathrm{s}$, $660 \, \mathrm{s}$ and $820 \, \mathrm{s}$), an I-pulse is missing. This is a limit of the CH instruments equipment software. To make a long NPV-experiment, several multistep experiments have to be combined into one macro. While the potentiostat automatically switches between multistep experiments, during a switch it does not record current. Therefore, the pulse-peak happens in the brief time in-between the two measurements and is not recorded.

AFM-measurements were done on a single line of the gold surface, as well as on a single spot. The single line measurements allow for nanomechanical mapping of forces, and the single spot measurements allow for a more precise measurement of the forces, i.e. a lower standard deviation. The next part contains the results for these two types of measurements.

### 7.2.1   Single spot: numerical values

In the AFM software, it is possible to control the movement of the X- Y- and Z-piezos. By setting the 'Slow Scan Axis' setting of the AFM to 'disabled', there will be no movement in the Y-direction. By setting 'scan size' to a low value, specifically $10 \, \mathrm{nm}$, the AFM will scan along a single line of this size in the X-direction (PFT oscillates in the Z-direction). In effect, the result is a single spot measurement. With these settings, an HSDC-file of force curves of a single spot can be obtained. Due to the low amount of topographical variation[13], we can obtain accurate numerical values for the probe–surface forces. Also, differences between different force curves due to different electrochemical conditions could be more noticeable.

SputterGold spot   Four measurement series were collected on the 'Sputter Gold' sample, one of which is from a single spot: the Sputter Gold spot dataset. The measurement scheme for this dataset is NPV with an increasing voltage in a potential range from $0.15 \, \mathrm{V}$ to $1.15 \, \mathrm{V}$. We made this sample using the sputter coater, which produces a lower crystal uniformity than the e-beam.

Figure 23a shows the average force–z_{height} force curves for the SputterGold-spot dataset. The average force–z curves are flat in the first part of the extension curve, the baseline.

---

[13]Grains in the gold layer, as shown in figure 7, cause this spatial variation.
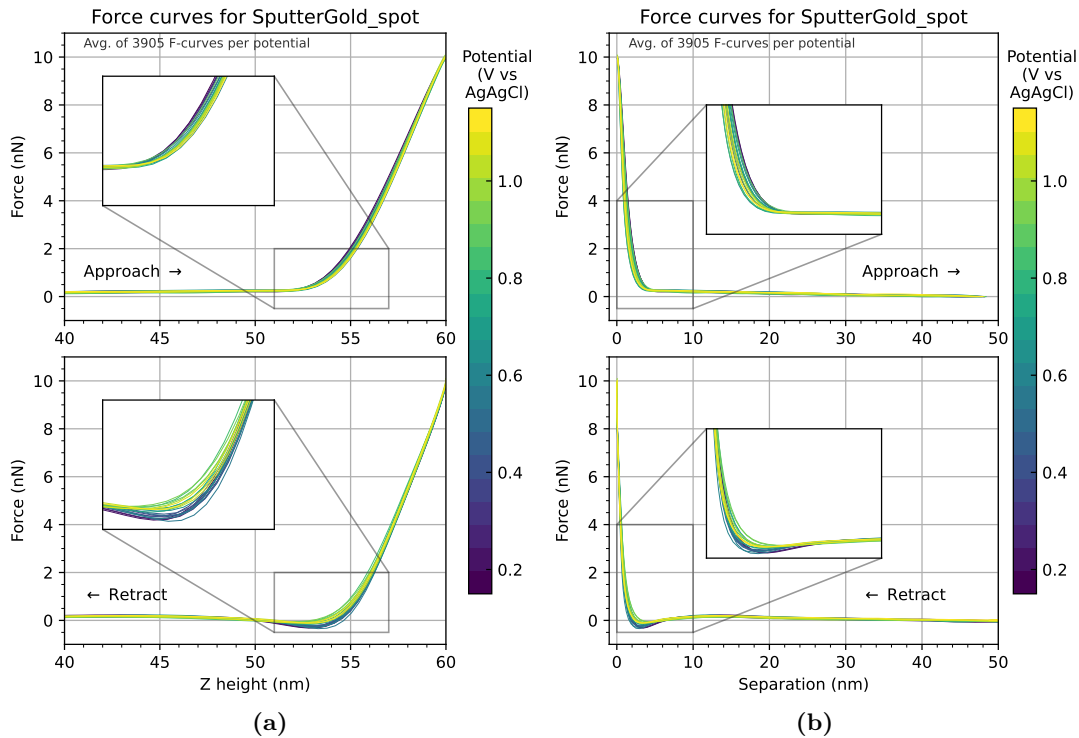
Figure 23 – Average force curves, with the approach in the top panels and the retrace in the bottom panels, of sample SputterGold-spot for all NPV-potentials (indicated by the color-bar) with a zoomed inset on a high-variation part. For the channels: (a) force–z, (b) force–separation.

Between 52 nm and 56 nm, the forces rise increasingly. This middle part of the force curve is where the tip is not yet in contact with the sample, and thus where the van-der-Waals and double layer-forces from § 2.2 play a role.

From 56 nm to 60 nm, forces rise in a straight line and the curves show linear deformation of the tip-sample system. In this region, the tip is in contact with the sample. The retract-curves show a small adhesion dip, of about 0.2 nm. Compared to the plot of theoretical forces, figure 2, a magnitude of around several times 0.1 nN is reasonable.

Figure 23b shows the average force–separation force curves for this sample for each potential, with the approach and retract part of the force curve separated. It shows stable force curves with consistency across potentials. The approach curves are almost, but not completely, flat until about 3 nm separation, where the forces start to rise. Forces reach a maximum value of 10 nm, which is how the peak force was set. Note that the range of the EDL- and vdW- forces in § 2.2 is about 5 nm. In the retract-curves, a clear adhesion dip of around 0.2 nm can be seen. The adhesion part of the force curves is the part where the voltage divergence is the largest. At larger separations, the retract-curves contain a small (0.1 nm) broad peak of positive forces – perhaps repulsive double layer forces – after the adhesion part, and the tails of the force curves are flat.

The curves in figure 24a show the z-derivative of figure 23a: $\frac{\mathrm{d}F}{\mathrm{d}z}$, the elasticity. We expect the derivative force curve to look similar to figure 24b, with two main regions in the approach curve, and three in the retract curve.

In the approach part, we expect two regions, one with zero elasticity and a plateau with a constant elasticity of about the magnitude of the spring constant of the cantilever (in this case $k = 1.5422 \, \mathrm{N/m}$). The measurement results roughly follow this form, but $\frac{\mathrm{d}F}{\mathrm{d}z}$ exceeds the k-value. Perhaps because the tip is indenting the gold surface, meaning the surface can not be assumed to be a rigid body. Also, while in the rough sketch of the expected
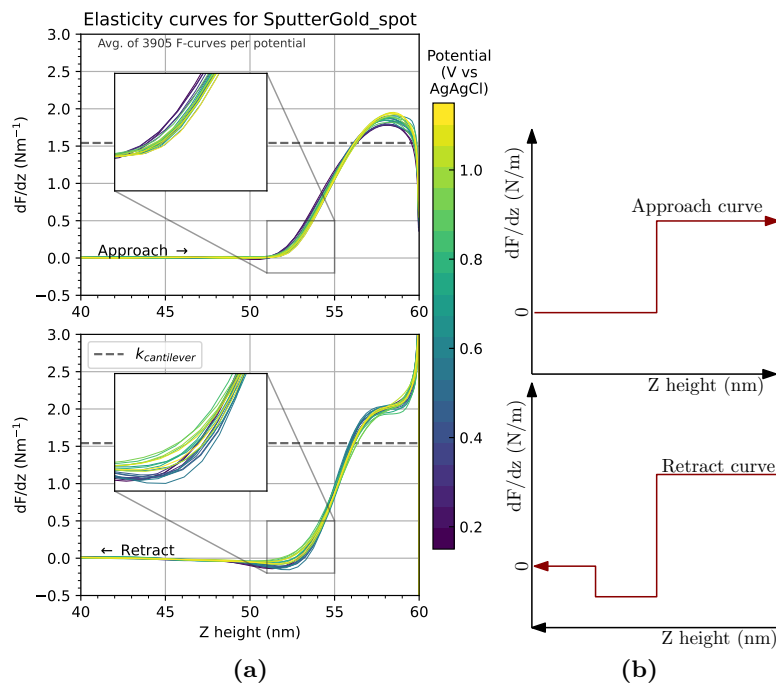
Figure 24 – (a) Average force curves of $\frac{\mathrm{d}F}{\mathrm{d}z}-z$ for sample SputterGold-spot. (b) Sketch of expected global $\frac{\mathrm{d}F}{\mathrm{d}z}$ curve shape.

elasticity the transition between the two regions is a step, in the measurement results the transition is smooth. This transition region between the baseline and the plateau is where the probe-surface forces are. In the plateau, the values for different voltages differ the most, which is about $0.2\,\mathrm{N/m}$.

In the retrace part, we expect three regions: a contact part with a value near the spring constant, an adhesion part with negative elasticity, and a baseline with zero elasticity. Like the approach, the measured curves have these regions, though with smooth transitions in-between. There is an adhesion dip at $53\,\mathrm{nm}$, which is small, and higher for lower potentials. Both approach and retrace curves contain a sharp deviation of elasticity in the last few nm, which is probably due to the cut-off between the two parts of the force curve, and not of physical relevance.

To ameliorate the cross-voltage analysis of force curves, figure 25 shows the force curves next to each other in a 2D coloured plane. Force is on the colour axis of a separation–potential plot. In Python, the plot is produced by interpolating the values to a grid[14] with `scipy.interpolate.griddata()` and plotting on that grid using `matplotlib.pyplot .pcolormesh()`. Each vertical slice of this plot is an average force–separation curve. The approach plot, which has a wide potential-range, shows little variation across voltages. Forces begin to rise at an onset-point around $2\,\mathrm{nm}$ separation, and at some potentials at a slightly lower separation. In the retrace-curves, the force-range is small ($\pm0.3\,\mathrm{nN}$), to show the adhesion. Between $2\,\mathrm{nm}$ and $5\,\mathrm{nm}$, a negative force band corresponds to the adhesion, which has a sharp maximum at $0.55\,\mathrm{V}$ vs. Ag/AgCl and a broad maximum at $0.2\,\mathrm{V}$. From $0.65\,\mathrm{V}$ onwards, the adhesion is lower, and the high-F onset point is at further separation. At separations beyond $5\,\mathrm{nm}$, there is variation of the positive forces across potentials.

The adhesion was also directly calculated, and for this sample figure 26a shows that it is low. At potentials below $0.5\,\mathrm{V}$, the average adhesion is around $0.3\,\mathrm{nm}$ and as expected for a single spot measurement the standard deviation is low, about $0.1\,\mathrm{nm}$. The peak in adhesion at $0.55\,\mathrm{V}$ to $0.6\,\mathrm{V}$ is clear again. At higher potentials, the adhesion is reduced,

---

[14]A new grid is needed because every average force curve has different separation values.
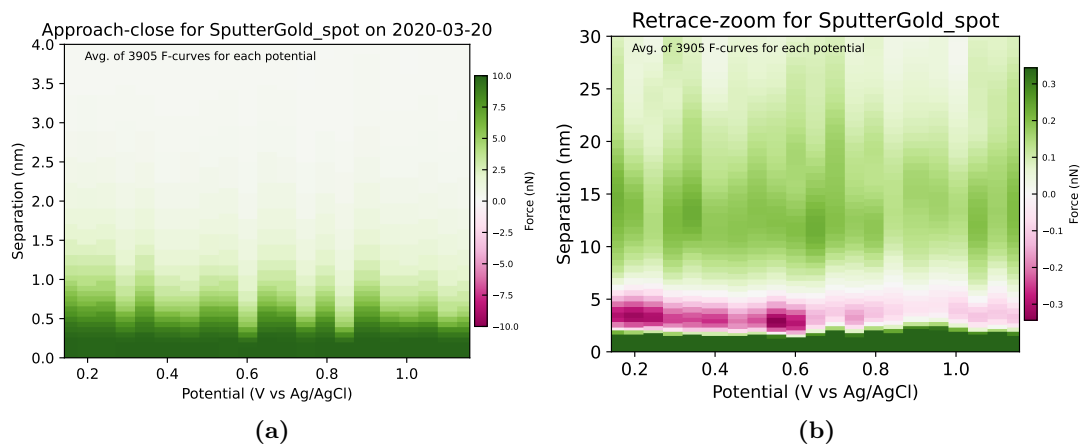
Figure 25 – SputterGold-spot plots of average force curves side by side in a separation–V 2D-plane with an F-colour axis for (a) approach with broad F-range (b) retract with narrow F-range.
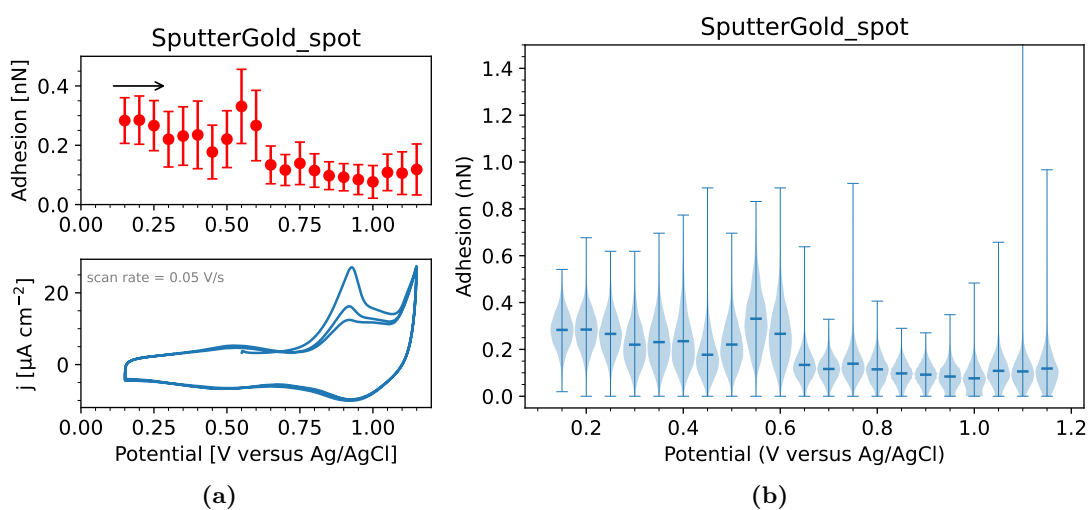
Figure 26 – SputterGold-spot plots of adhesion of all force curves per potential: (a) combined plot of average adhesion with standard deviation and a CV with scan rate 50 mV/s. (b) violin plot, where shape-width corresponds to the frequency of an adhesion value.

to around 0.1 nm with a standard deviation of 0.05 nm.

Figure 26a also shows the CV of the SputterGold sample, that we compare to CVs in literature as described in § 2.4. This CV contains an upward oxidation peak at 0.92 V (O_2-adsorption or sulfate ordering), and a broad downward reduction peak at 0.91 V (O_2-desorption). At 1.08 V the current starts to increase sharply (start of second oxide adsorption peak). A less pronounced reduction-oxidation peak-pair is seen around 0.5 V. What is the relation between the CV and the features in the adhesion? Peak adhesion occurs in the double-layer charging region that lies approximately between 0.3 V to 0.8 V. Since this dataset used an increasing NPV experiment-scheme, we should look at the top lines of the CV. It seems like the peak adhesion corresponds to the oxidation peak at 0.5 V, and that the low-adhesion, low standard deviation values appear after this (oxidation) peak is finished. This could be related to sulfate adsorption and double layer charging. Oxides are adsorbed for the three adhesion values of 1.05 V and higher, and it seems that at these potentials the adhesion slightly rises by 0.03 nN.

For further analysis of the adhesion distributions, figure 26b shows a violin plot of adhesion versus potential for this dataset. At each potential, the distribution of the adhesions is shown including its extrema and mean. For the SputterGold-spot measurements,

the distributions are centred around the mean adhesion. In accordance with the lower standard deviation, above 0.6 V the distributions are narrower than below. At 1.1 V, there is a large maximum adhesion in the distribution. This maximum value belongs to one force curve and is likely caused by an external vibration that was detected by the AFM.

Integrating the electrochemical pulses of figure 21 yields the total charge that flowed during each potential pulse. In figure 27, the blue lines show the charge that flowed during the pulses after the potentiostat switches from V_{base} to V_{pulse}. The orange line shows the charge after returning to the base voltage. The lines are of opposite sign with
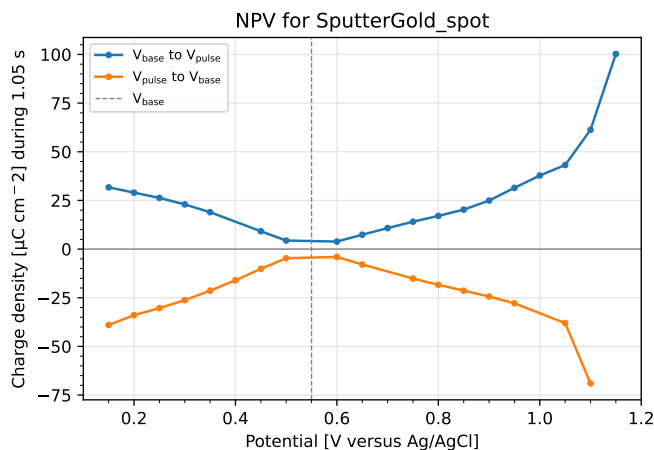
Figure 27 – NPV plot for SputterGold-spot, showing the integrated current for each pulse, which is a cumulative charge density during 2 s. It contains the base-to-pulse charges (blue) and the pulse-to-base charges (orange).

equal magnitude, forming an 'X'-shape: the charge decreases from an absolute value of $40\,\mu C/cm^2$ at low potentials to almost zero near the base-voltage, at higher potentials it increases – above 1.1 V with a higher slope, cf. the CV – until $100\,\mu C/cm^2$.

WaxGoldTi May   The same HSDC-measurements were performed on the sample 'Wax Gold Ti', which differs from the 'Sputter Gold' sample in that it has a Ti- instead of a Cr-adhesion layer, and that it has wax as an insulator instead of nail polish. Again, an increasing NPV measurement scheme was used on a single spot. We collected this dataset in May 2020. In figure 28a, the average force–separation curves are clean, with a peak force of 10 nN and a broader range on the x-axis due to a higher peak force amplitude. The F–Z-plot is omitted because the separation plot is more useful. The forces curves vary little across potentials, and the baselines have a broad positive force-peak of 0.2 nN high. The retrace-curve has an adhesion dip of 0.35 nm and slightly 'boomerangs': in the contact part the separation increases slightly. This could be due to improper deflection sensitivity calibration[15].

The $\frac{\mathrm{d}F}{\mathrm{d}z}$-plot of figure 28b shows that in the approach curve, the maximum elasticity is the value of spring constant k. In the retrace curve, the spring constant is at the point where the inflection between the rising part and the plateau happens. This plateau is not horizontal but sloped. The elasticity curves have a clear voltage dependency. At low potential in the retract-curves, the rising part is less steep, and the plateau is lower.

The separation–V–F 2D plots illuminate some potential-dependencies that are not visible in the scatter plot (figure 28). Figures 29a and 29b show the approach curves focusing on the contact-range (narrow separation of 0 nm–10 nm, broad F of 0 nN–10 nN) and

---

[15]Even though the retrace part of the force curve is already the one that is used for the deflection sensitivity calibration. This can be fixed by adjusting the $k_{threshold}$.
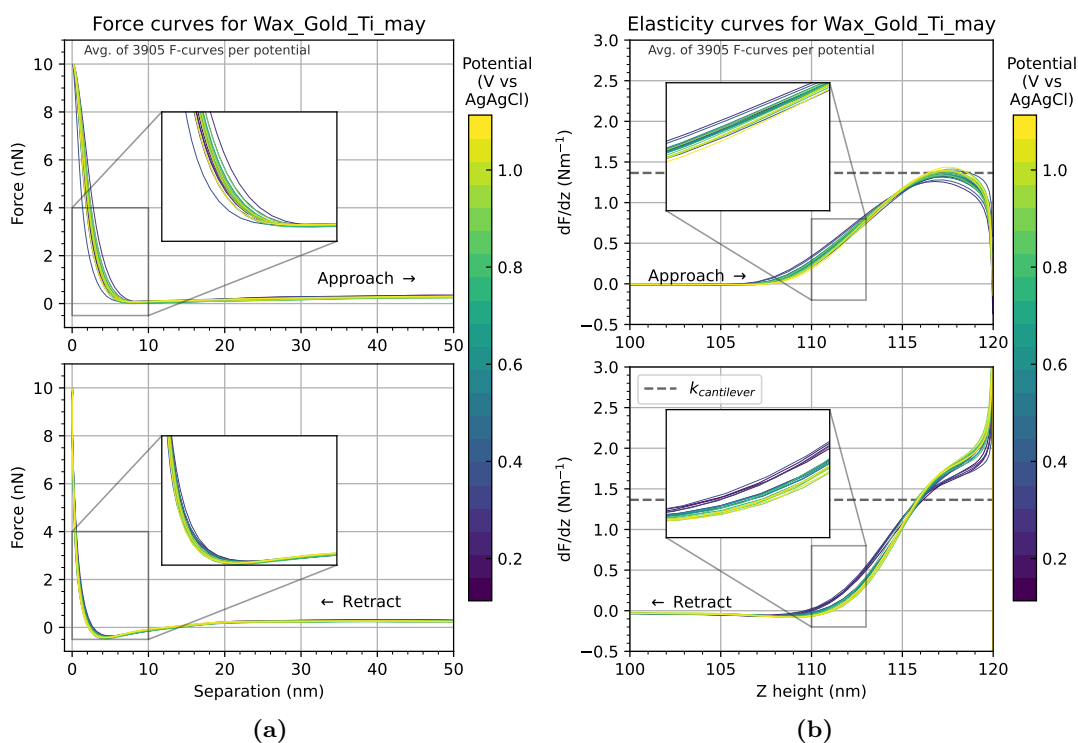
Figure 28 – Average force curves for sample WaxGoldTi-May showing channels: (a) average force–separation, (b) average dF/dz–z.

the entire range (broad separation of 0 nm–100 nm and narrow F of -0.3 nN–0.3 nN) of the force curve, respectively. In the contact range, the onset point starts at a higher
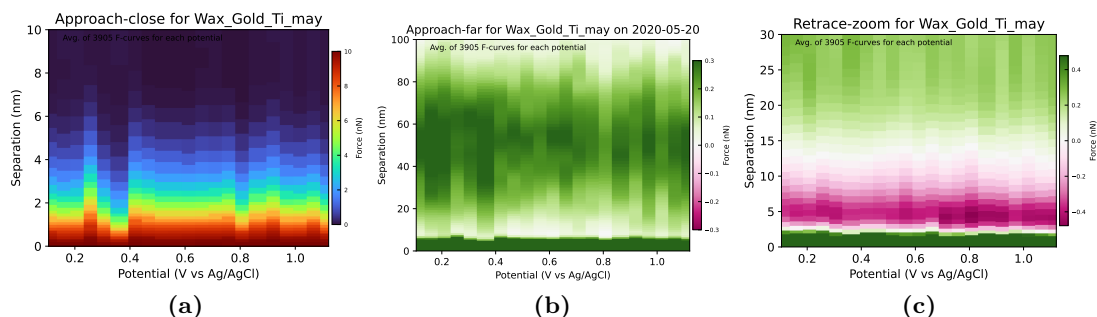
Figure 29 – WaxGoldTi-may plots of average force curves side by side in a separation–V 2D-plane with an F-colour axis for three parameters ranges: (a) approach in the contact part, where another colour map was used for clarity, (b) approach with a broad separation-range (c) retract with a broad separation range and a narrow F-range.

separation at 0.25 V, and at a lower separation at 0.35 V and 0.8 V. In the whole range, the slight positive long-range forces are visible (slightly less at 0.8 V). However, there is a lot of fluctuation and the magnitude of these forces is small, so since the variation across potentials is not much larger than the standard deviation of the force curves (~ 0.1 nN), any variation could just be noise. The retract-curves, as shown in figure 29c, show an adhesion band with a maximum value at 0.8 V.

The adhesion for WaxGoldTi-may is, at 0.4 nm, higher than for SputterGold-spot, as shown in figure 30a. The adhesion has a standard deviation of around 0.05 nm, making this an accurate spot-measurement. At 0.7 V, the adhesion is the highest, and there is a dip at 0.5 V. Cyclic voltammetry shows only a reduction peak at 0.5 V, and an onset of high current beyond 1.1 V. Integrated NPV-results, as shown in figure 30b, show that less current flows than in the SputterGold-spot dataset, but with a similar X-shape.
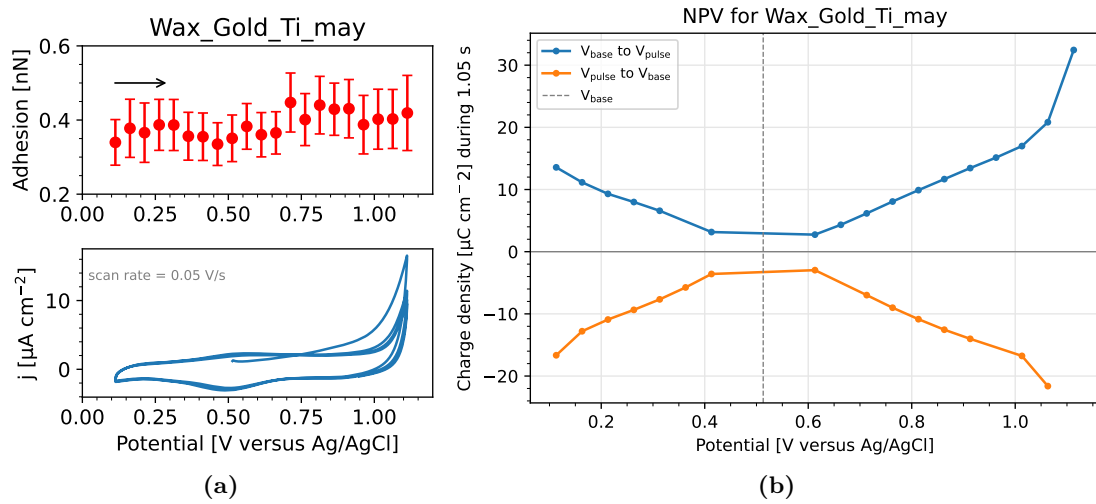
Figure 30 – Two plots for the sample WaxGoldTi-may. (a) Average adhesion versus potential (top), CV with scan rate 50 mV/s (bottom). (b) NPV integrated current versus potential.

WaxGoldTi June   In June 2020, we collected a second dataset on the WaxGoldTi-sample using increasing NPV on a single spot. While the sample is the same, the results are not the same. This is not surprising, since this measurement was performed on a different spot. Figure 31a shows the average forces curves. Compared to the measurement
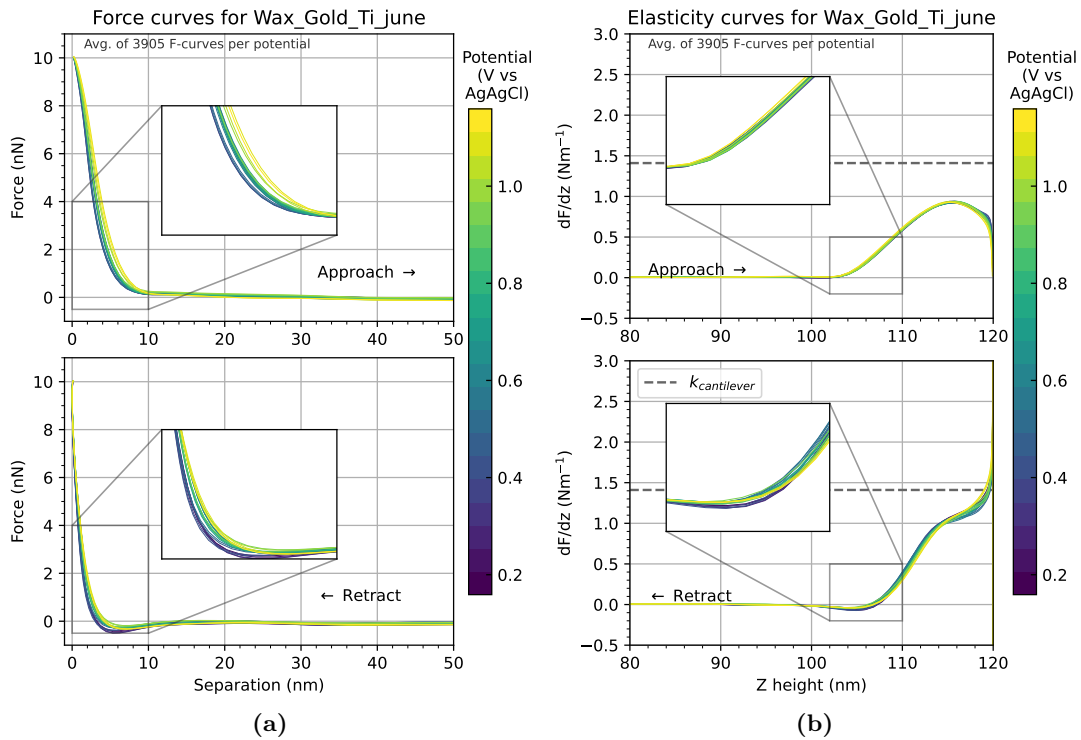

Figure 31 – Average force curves for sample WaxGoldTi-June, showing two channels: (a) force–separation, (b) elasticity–z-height, where dF/dz is the elasticity.

from May, these approach curves have no broad positive F-peak in the tail. The force curves are smooth, as expected for a spot-measurement.

The elasticity lines in figure 31b have a flat plateau at 1 N/m which is below the spring constant $k_{cantilever}$. This is unexpected, and perhaps a result of an incorrect spring constant calibration.

The 2D separation–V–F colour plots (figure 32) show that between the different potentials

of the WaxGoldTi-June measurement, the shape of the force curves changed noticeably. There are two areas in both the approach and the retract plot where the force curves
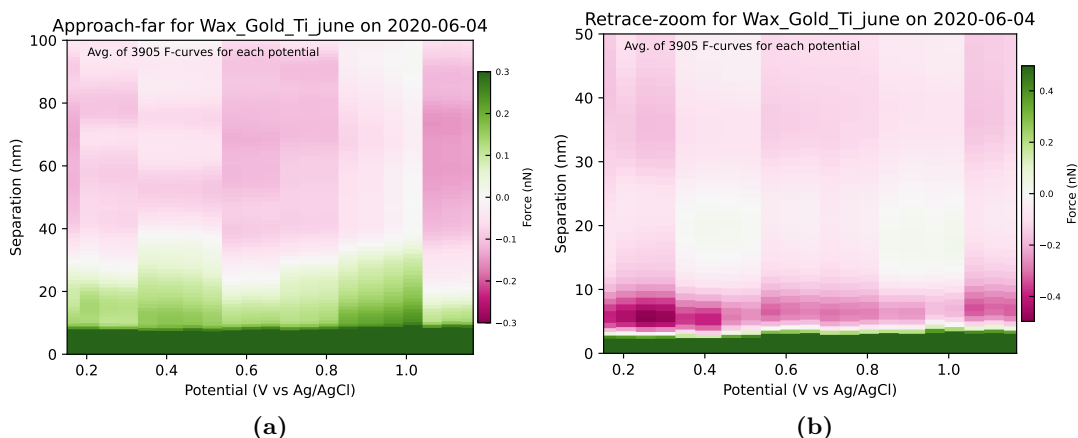
Figure 32 – WaxGoldTi-June plots of average force curves in a separation–V 2D-plane with an F-colour axis for the (a) approach, (b) retract.

deviate from the rest: at 0.35 V–0.5 V, and at 0.85 V–1.0 V. In the approach plot in this region there are repulsive (positive) forces that extend 20 nm further than elsewhere. In the retract-plot, the forces are also higher in this region – less negative. While it seems like the entire force curves are shifted upwards at certain potentials, we think this is not the case, because before averaging, the force data is subtracted with its minimum. At 0.3 V, there is a peak in the adhesion.

This peak is also observable in the violin adhesion plot in figure 33b, where there is a clear, broad peak (0.3 nm) in adhesion centred around 0.25 V. Adhesion drops at 0.45 V
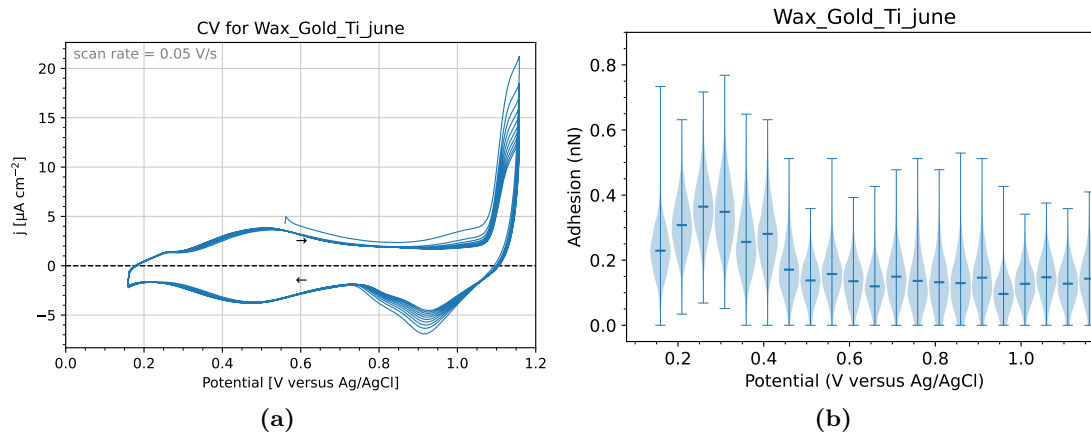
Figure 33 – Two plots for sample WaxGoldTi-June. (a) Cyclic voltammogram with 10 cycles and scan rate 50 mV/s. (b) Violin plot of adhesion versus potential.

to a value of 0.15 nm with standard deviation of around 0.05 nm; this measurement is accurate. There also is a slight dip in adhesion around 0.95 V. The adhesion-distributions are slightly bottom-centred.

The cyclic voltammogram shows an onset to high current (overall higher current than the WaxGoldTi-May experiment) beyond 1.05 V, and a reduction peak at 0.9 V, a smaller, broad reduction and oxidation peak around 0.45 V. This CV contains many (10) cycles, which illustrates how the peak height decreases per cycle as expected [46].

As earlier mentioned, the trends in the adhesion are different from the other measurement of the same sample. Besides it being different spots, one explanation for the difference

between the two measurements could be: for WaxGoldTi-may the reference electrode voltage was 113 mV, and for WaxGoldTi-June it was 159 mV. When the reference voltage is different, it causes the voltages that the potentiostat applies to map to different resulting potentials – in this case, the difference is 0.05 V. More concrete: the maximum voltage of the June-measurement was 0.05 V higher, and as a result this measurement includes a larger part of the oxide-adsorption peak. That is why figure 33a has the corresponding oxide-reduction peak and figure 30a does not.

We have seen that there is a variation in the forces between two different spots. In the next part we will see that by measuring an array of spots (a line), we can *map* forces.

7.2.2   Line scanning: nanomechanical mapping

In a single spot measurement, setting the X-scan axis scan-size to a low value allows for accurate results uninfluenced by topographical fluctuations of the gold layer. However, this topographical fluctuation can also be used to map the nanomechanical forces. It is interesting to see if changing the electrochemical conditions influences different sites in the gold layer differently.

By setting the scan-size to a large value (1 μm) we conduct a line-scanning experiment.

Nailpolish Gold 8jan   On the sample 'Nailpolish Gold 8jan', such a line scanning measurement was carried out. This sample was made with E-beam lithography, and for the measurement increasing NPV was used in a potential range of 0.10 V–1.10 V.

The results of this measurement show variation in the average force curves for different potentials (figure 34b), most clearly in the adhesion (see figure 34a). The average adhesions
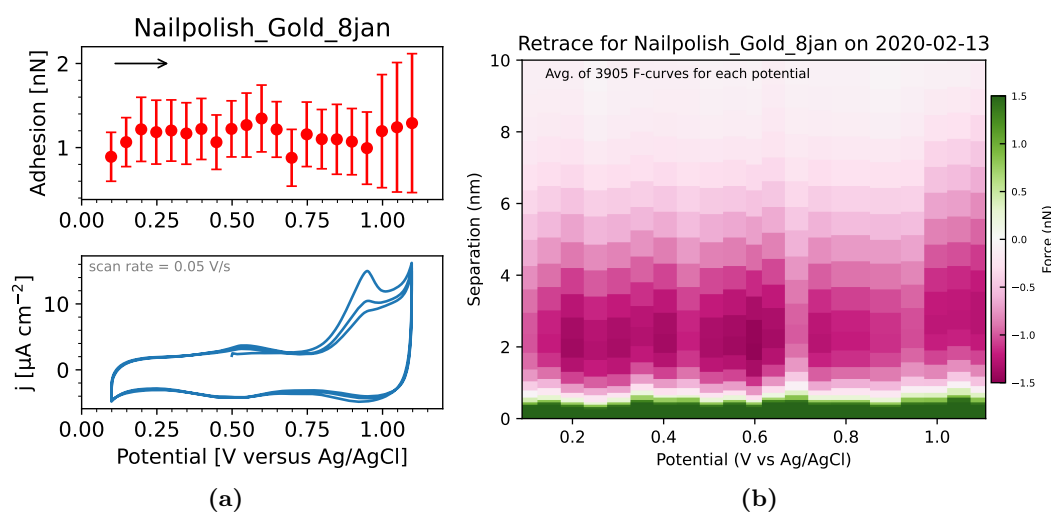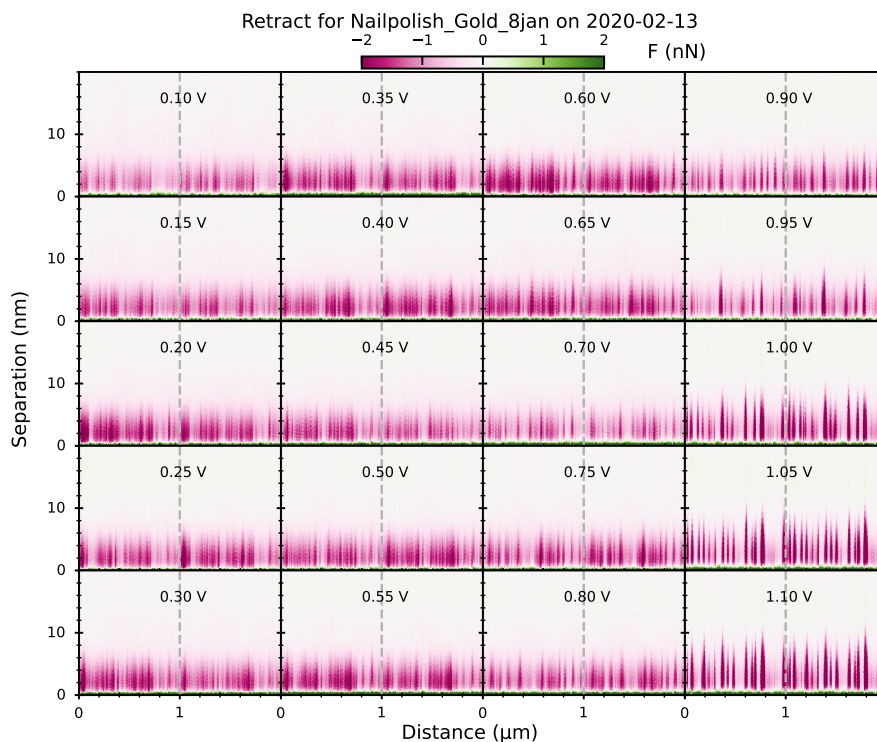

Figure 34 – Two plots for sample Nailpolish Gold 8jan. (a) Adhesion and CV. The data of 0.85 V required dropping some noisy force curves, due to vibrations by a closing door. (b) Average force curves, the retrace part, in a separation–V 2D-plane with an F-colour axis, with a narrow separation range of 10 nm.

for this sample in figure 34a are large – around 1 nm – with a large standard deviation of about 0.3 nm. At the lowest voltages, there are lower adhesions, and there is a dip in adhesion at 0.45 V, and 0.7 V. Above 1 V, adhesion starts increasing with a clear increase in the standard deviation. In the CV, we see an oxidation peak at 0.95 V, matching a reduction peak at 0.92 V, and another peak-pair at 0.53 V (oxidation) and 0.49 V (reduction). Moreover, there is the start of a peak at 1.05 V.

The average force curves, in the colour plot of figure 34b show an adhesion-region between 1 nm–5 nm separation. It shows the same characteristics for the adhesion as described above, including a low adhesion at 0.7 V and 0.9 V, and an adhesion maximum at 0.6 V. The adhesion reaches higher separations at ≥ 1 V. We see that for a line-measurement, like a spot-measurement, the potential influences the forces. However, the standard deviation is higher and the measurement is less accurate than for a spot.

Is the found influence of the electrochemical conditions on the average adhesion homogeneous? The increase in standard deviation at higher potentials in figure 34a suggests otherwise. This is strengthened by the violin plot, figure 42 in appendix A.5, where at these high potentials, the bulk of the adhesion decreases, while the maximum adhesion increases.

Here, the line-scanning allows for deeper analysis – by making a topography plot. This plot (figure 35) shows all force curves (non-averaged) of an HSDC-measurement next to each other, horizontally arranged. In this plot, with distance (along the X scan-axis) on the x-axis and separation on the y-axis, the force is displayed with a colour axis. For each potential, such a plot is made, and this potential-dimension is visualised either by chaining the plots in an animation, or – as is shown here – by arranging the plots in a grid of plots. When using a colour axis, the visible features of a plot can vary depending on

Figure 35 – Force curve map, showing all retrace force curves plot for the sample Nailpolish Gold 8jan. The distance in μm is the distance along the X scan axis. Each panel is the full HSDC measurement at a potential. The grey dashed line marks the two scan lines.

the plot-ranges and settings. The plot is more insightful when the plot-range corresponds to the region where the data varies the most. In this case, we used a normal F–separation plot to find an appropriate range for the force and the separation. Generally, for these kinds of plots, the interesting ranges are either broad F with narrow separation (the steep part of the force curve) or narrow F with broad separation (the baseline including the adhesion). The shown plot uses the latter.

Furthermore, this plot uses flipped line correction, because not every measurement started out in the same scanning-direction. During an HSDC-measurement, the AFM-tip scans several times back and forth along a line on the surface – how many times depends on the tip velocity. If we want to compare topographical features between different lines, all lines need to point in the same direction. Therefore, all odd lines are flipped in a dataset that started scanning to the right, and in a dataset that started scanning to the left all even lines are flipped.

This retrace-plot contains two lines per plot, and NPV with increasing potential. The force-profile between the two lines of one plot is almost identical, while the force profiles of different plots are similar – the spikes in the adhesion remain at the same distance-position. This shows that the data analysis method is adequate for mapping topographic features.

While similar, there are differences in the force profiles of different plots – after all, the electrochemical conditions are different. The clearest difference is in the adhesion: at

$\geq 1\,\mathrm{V}$ some spots obtain a larger and further extending adhesion. That is where the increased standard deviation and maximum of the adhesion in the previous plots come from. Certain locations have high adhesion, and these high-adhesion spots remain the same at different potentials. We suspect that these high-adhesion spots are related to localised electrochemical processes, specifically oxide adsorption, as described in § 2.4. The spots are about 15 nm wide, which is similar to the grain width shown in the topography (figure 36a) – so gold structure could also play a role.

Topographical features in the force curves can only be related to the structure of the gold layer if that stays constant. The height-map of figure 36a shows that this is the case. This height map uses height-sensor data[16]. Height-sensor data needs to be
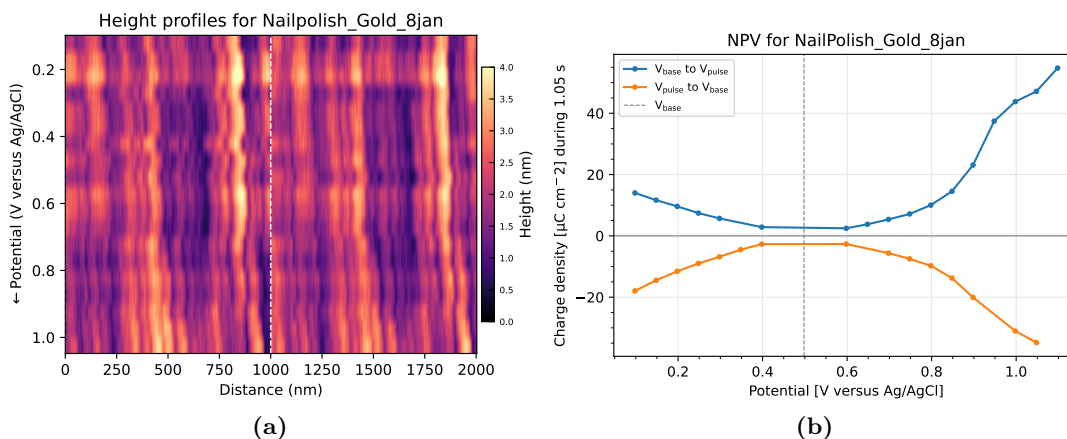
Figure 36 – Plots for the Nailpolish Gold 8jan sample. (a) Height–distance plot for each potential, with flipped line correction applied, and in the centre a dotted line indicating the different lines. (b) Integrated current versus potential plot.

corrected before it can be interpreted, so we perform a 0th and a 1st order correction using `scipy.signal.detrend()`. There is some drift, yet only $\sim$50 nm, so overall the topography was constant during the NPV experiment. The NPV charge plot of figure 36b is slightly asymmetric at higher voltages, with higher charges at the positive side.

SputterGold increasing   For the 'SputterGold'-sample, in addition to the earlier described spot-measurement, we performed three line-measurements. One NPV measurement with increasing voltage in the range 0.15 V–1.15 V, one with decreasing voltage in the same range, and one with increasing voltage in the range 0.85 V–1.05 V; each for 21 voltages. In figure 37a, multiple CV's show that if the range is until 1.15 V (blue and orange lines) the sulfate ordering peaks at 0.9 V dominate, and that if the range is until 1.25 V (green line), the oxide adsorption peaks dominate (shown by the oxide-reduction peak at 0.9 V). Therefore, the range of these measurements implies mostly adsorbed sulfates and not many adsorbed oxides.

In figure 37c we see that for the increasing V-measurement, the adhesion is around 0.2 nN with only a slight potential-dependence: at higher potentials, the adhesion is $\sim$0.1 nN lower. This dependence is similar to the spot-measurement for the Sputtergold sample (figure 26b), but less pronounced. At 0.15 V and at 0.7 V, the adhesion peaks, which is also clear in the colour plot of the average retract curves of figure 37d. From around 10 nm to 30 nm there is a slight repulsive force in the force curves.

For this dataset, we also made a force curve map showing all retrace force curves next to each other, figure 38, to study local variation. In this measurement, the AFM scanned

---

[16]The NanoScope software provides two types of topography data channels: height and the more raw height-sensor. The difference is that height-sensor data includes the sine wave of PFT, and height-data does not.
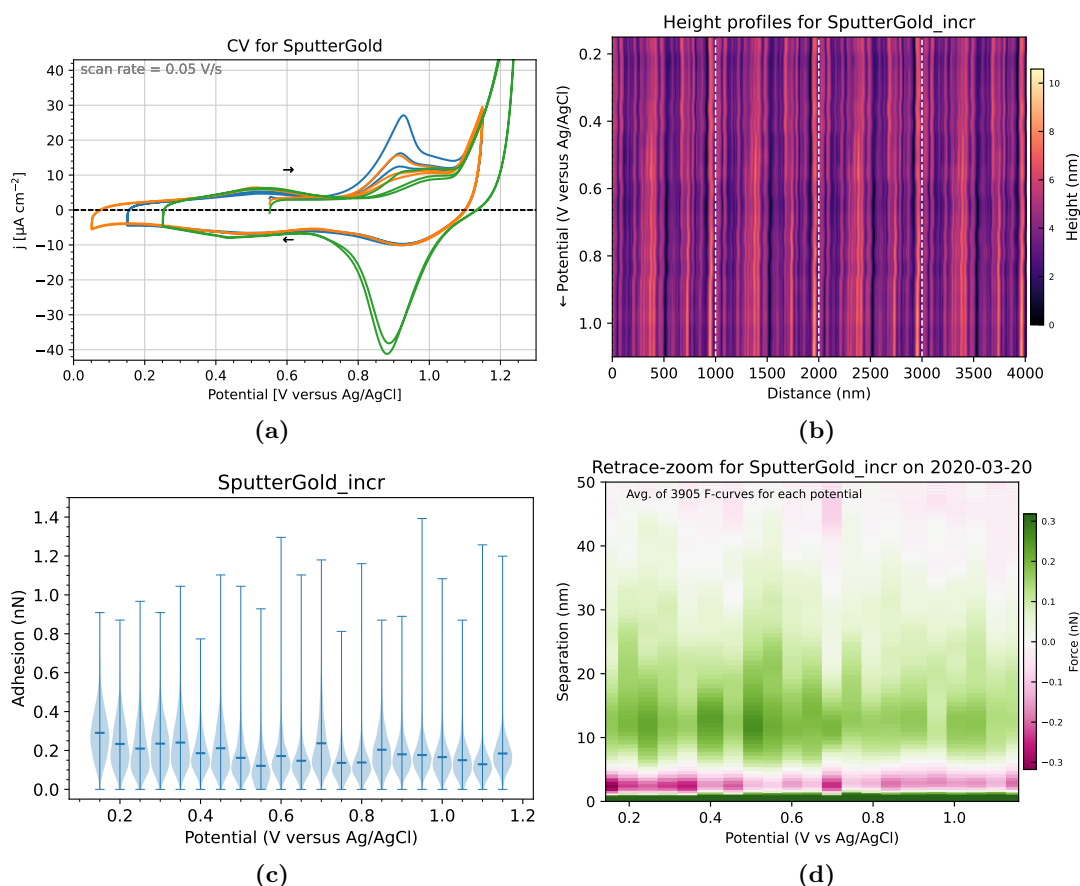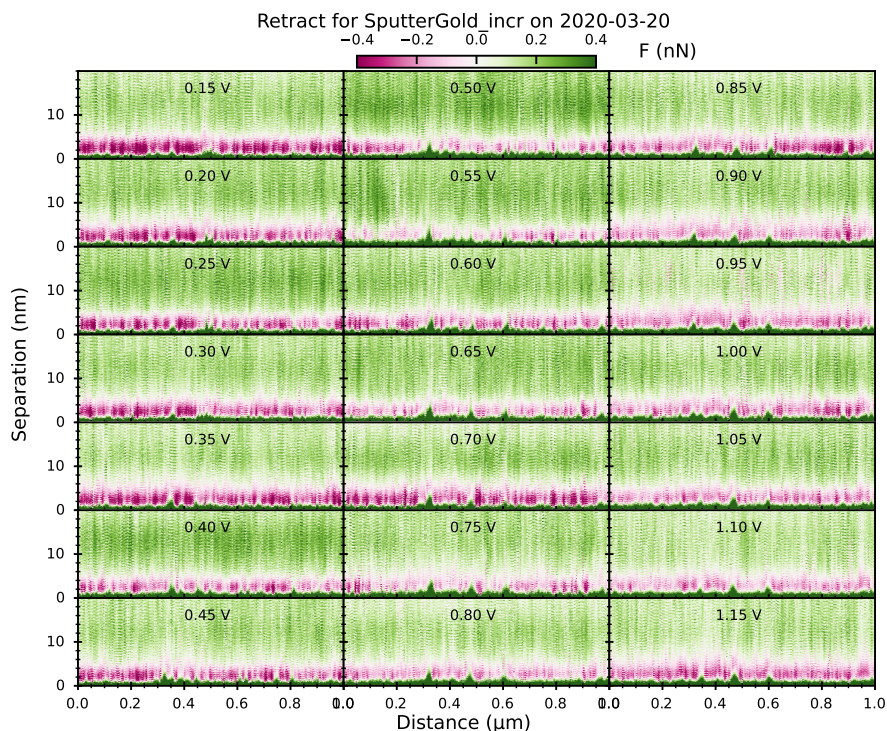
Figure 37 – Plots for the Sputtergold-increasing dataset. (a) CV of the Sputtergold sample with scan rate 50 mV/s. (b) Height–distance plot of four times the same line, with dotted lines marking the four scans of that line. (c) Violin plot of adhesion–potential.

back and forth two times, resulting in four times the same line, as the height plot shows (figure 37b). The topography remains constant throughout the measurement. For figure 38 however, we selected one line (the leftmost) for clarity. Because the shape of the plot is similar across the four lines – indicating reproducibility –, this line is representative. In the force curves, there are green 'spikes' (for example at 600 nm at 1.15 V) where the repulsive force extends further than elsewhere. These spikes occur at the same locations at several potentials, though they gradually change. Adhesion is also localised, i.e. higher at some locations than others. But compared to figure 35, this effect is less pronounced – as the adhesion is lower.

SputterGold decreasing   To find the influence of the voltammetry scheme, we repeated the previous measurement, but with decreasing potentials – so the first pulse was 1.15 V, and the last 0.15 V. I will proceed to the adhesion, because the CV is the same as for the previous measurement, and the height plot is similar. In figure 39a, the adhesion is around 0.2 nN for potentials $\leq$0.4 V, and around 0.15 nN above this potential, with a minimum at 0.8 V and a peak around 0.9 V. This also shows up in figure 39b, where, additionally, bands of repulsive forces are visible around 0.4 V and 0.8 V.

In the force curve map for this dataset, figure 39c, the general shape is the same as for the increasing V-measurement. When we compare the locations of the adhesion peaks (which we can do, because the same line was scanned), these turn out to be not the same.

As mentioned, we observe that there is no large difference in the potential dependency of the increasing and decreasing V-measurement. Initially, we expected that increasing V would link with following the upper (oxidation) part of the CV, and decreasing V

Figure 38 – Force curve map, showing all retrace force curves for the dataset Sputtergold increasing. The distance in µm is the distance along the X scan axis. This plot only shows the first scan of four scans of the same line.

with the lower (reduction) part, thus causing different electrochemical conditions. This thought was erroneous, because NPV works with pulses. Thus, every AFM measurement is conducted during a reduction or oxidation pulse, depending on whether V_{pulse} is respectively lower or higher than V_{base}. Accordingly, we can interpret the increasing and decreasing V-measurements as experimentally identical.

SputterGold zoom   The final variant of the experiment is zooming in on a subset of the potential range. Because of the oxide-reduction peak at $0.9\,V$, we chose a range of $0.85\,V$–$1.05\,V$ and consequently here $\Delta V = 0.01\,V$. Of course, with the previous discussion in mind, the oxide-reduction peak is not crossed in the measurements, but the oxide-adsorption peak is.

Figure 40 shows the results for this measurement. What stands out, is a peak in the adhesion at $0.9\,V$, where there simultaneously is an oxidation peak in the CV that is related to either sulfate organisation, or oxide adsorption. However, if these processes affected the adhesion, it would be more logical that the adhesion below $0.9\,V$ would be different than above – instead of only a peak at $0.9\,V$. It is unlikely that the peak in adhesion is related to current dynamics because (i) in the integrated current plot there is no deviating value at $0.9\,V$ and (ii) the AFM measurements are done several seconds into the pulse, when the current has already flowed.

To provide some final remarks about the results, a difference between increasing and decreasing potential measurements – which was not found – could be found with staircase voltammetry, albeit in a narrower V-range. Moreover, from the data more nanomechanical properties could be extracted, and maps of for example the elasticity could be made.

(a)

(b)

(c)
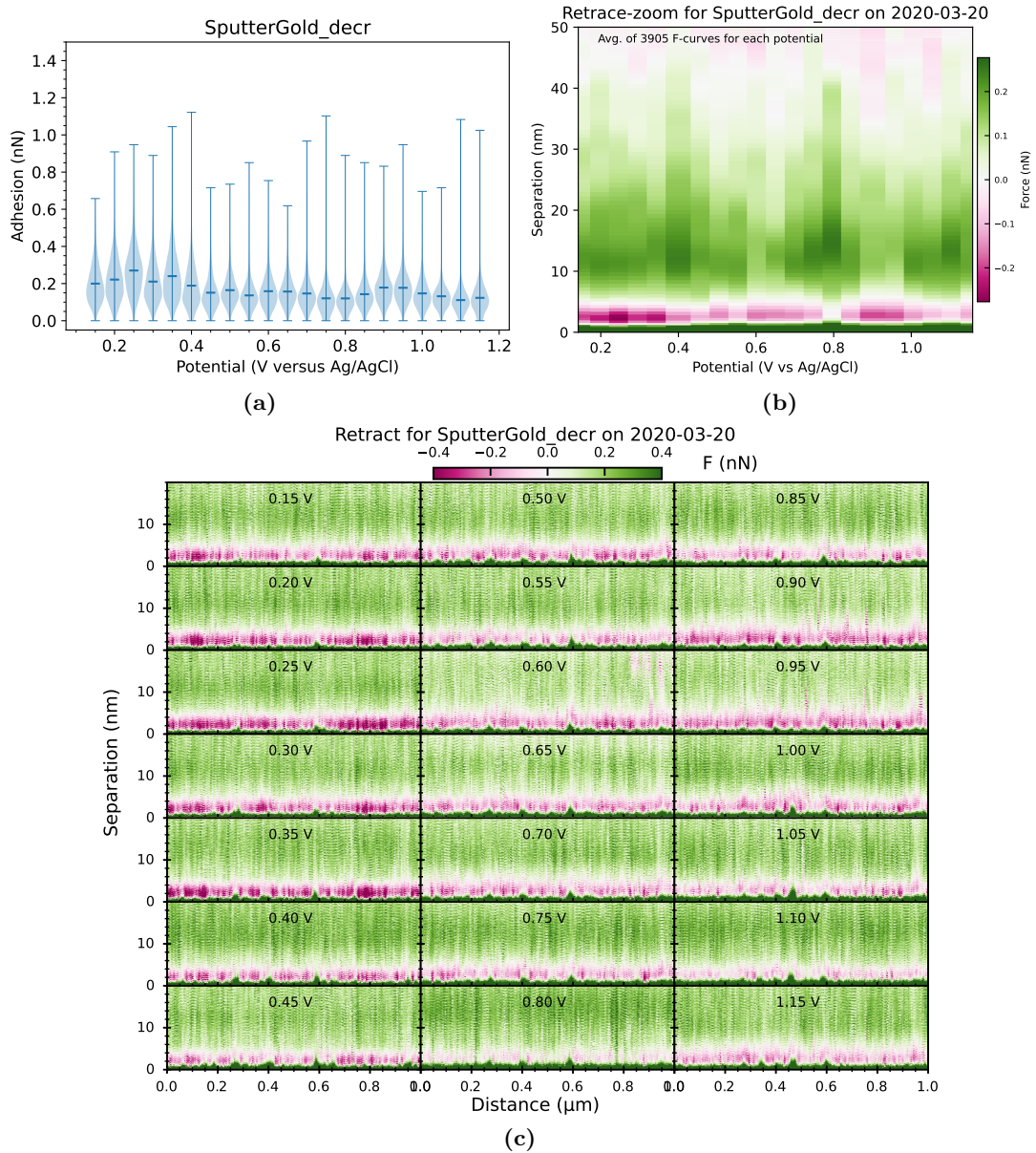
Figure 39 – Plots for the Sputtergold decreasing dataset. (a) Violin plot of adhesion–potential. (b) Average force curves in a separation–V 2D-plane with an F-colour axis. Shown is the retrace-part of the force curves with a narrow F-range. (c) Force curve map, showing all retrace force curves. This plot only shows the first scan of four scans of the same line.

(a)

(b)

(c)
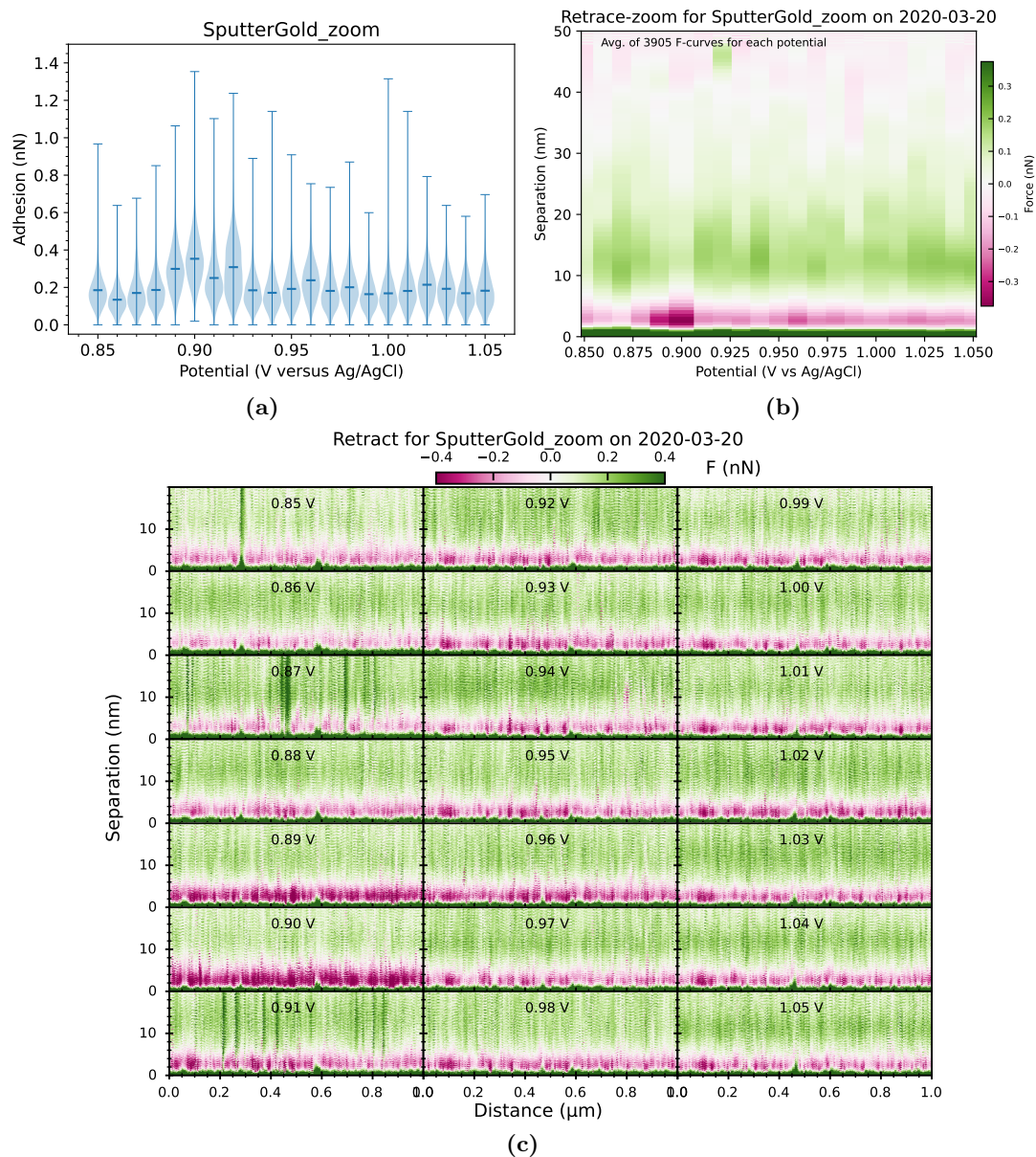
Figure 40 – Plots for the Sputtergold zoom dataset. (a) Violin plot of adhesion–potential. (b) Average force curves in a separation–V 2D-plane with an F-colour axis. Shown is the retrace-part of the force curves with a narrow F-range. (c) Force curve map, showing all retrace force curves. This plot only shows the first scan of four scans of the same line.

8 Conclusion and outlook

Summing up, in this thesis I demonstrate electrochemical AFM measurements with the aim of measuring heterogeneous electrochemical processes at the solid–liquid interface. With the results from the normal pulse voltammetry measurements using the custom data analysis method, we can draw the following conclusions regarding the research questions. Firstly, in several measurements, we find a clear dependence of the forces on the potential of the gold electrode. Secondly, this dependence is the most notable for the adhesion, and – as hypothesised – close to the surface, although the relation between potential and adhesion varies per dataset. Based on our data, we can not conclude that the elasticity is a good gauge for the electrochemical state in our experimental context. The data shows some indications for a potential dependency of long-range repulsive forces, but not as eminent as the adhesion. Thirdly, we think that our experiment and data method allow for *in-situ* mapping of the forces near the gold surface. Adhesion is observed to be spatially inhomogeneous, in addition to voltage-dependent. Therefore, our results suggest that adhesion can map localised electrochemical processes.

However, the results lead to several questions. There is an order of magnitude difference in the adhesion measured on substrates made with e-beam lithography and sputter coating. This is possibly caused by a difference in surface roughness (and thus surface area), a quantity that could be calculated from AFM topography images [51].

Moreover, the explanation for the locations of the high-adhesion spots is still unclear. It could be related to the topography, as the locations remain the same across different pulses during a normal pulse voltammetry experiment. In between each pulse, the system in principle equilibrates at the base potential. This relation to the topography could be indirect, i.e. that the adhesion is caused by local sulfate/oxide adsorption, which for some reason preferentially happens at certain locations. It could also be that the adsorption is randomised, and that the system did not fully equilibrate in between pulses.

Another question is the uncertainty in the separation values in the force curves. After contact with the surface, the quick detachment of the AFM tip might, in combination with the high tapping frequency, distort the separation values. Separation values are highly sensitive to the deflection sensitivity value. That is why we correct this value for each force curve, but the part of the curve we choose for fitting matters, so perhaps better parameters can be found. The force is not a function of deflection sensitivity, but it depends on the spring constant, which could also be more accurately determined [52].

Finally (regarding the questions), the used AFM method makes it difficult to pull apart the different parts – double layer, van der Waals and solvation – of the forces [21] without varying experimental conditions.

Consequently, this provides inspiration for further research. Van der Waals forces can be enlarged by using a larger tip radius, double layer forces can be affected by the ion concentration and the potential. Experiments varying these parameters can for that reason help in differentiating the force components. In addition to the potential we apply between the electrodes, our experimental setup also allows potential control over the tip, which would be interesting to use. Furthermore, the accuracy of the AFM force measurements can be verified by comparing the force curves from peak force tapping to single ramp force curves.

From the data of the reported – and future – experiments, we can extract more information by expanding the data analysis method. Simple first steps are making a map of the adhesion, and of elasticity. More advanced is fitting different contact mechanics models to each force curve and extracting more nanomechanical properties (deformation, DMT modulus, dissipation). For this, we would need to measure the tip radius, know the tip geometry, and match the assumptions of the model to these and further parameters.

While our data analysis method works and is flexible, it might be worthwhile to try out different software. Appendix A.3 lists alternatives, of which I recommend writing an HSDC reading extension for Gwyddion.

Regarding the electrochemical techniques, I recommend matching the experiment mode to the potential range. Despite the bubble issues we encountered, staircase voltammetry can be useful for probing both the top and bottom lines of the cyclic voltammogram, when used in the (sulfate adsorption and double layer charging) potential range between 0.3 V and 0.8 V. Pulse voltammetry is useful for the higher oxide adsorption potentials, and by collecting AFM data *after* the pulse too, the reduction behaviour can be measured. As our solution comparison in section 6 shows, other electrolytes such as salt display V-dependence of adhesion.

Lastly, to better relate the results to the structure at the gold–solution solid–liquid layer, and compare this to theory, it is a good idea to use single-crystal gold substrates. And, to measure the composition using X-ray diffraction. In principle, with a better understanding of EC-AFM, the technique can be applied to study the applications of electrochemistry such as catalysts and batteries.

A   Appendices

A.1   Acknowledgements

A.2   Experimental details

The following specific experimental devices were used for the experiment:

- AFM table stable: Herzan TS-140 +40

- AFM tip: Scanasyst Fluid, triangular geometry, Si_3N_4, tip radius $20\,nm$, resonant frequency $150\,kHz$, length $70\,\mu m$, spring constant $k = 0.7\,N/m$, all 'nominal' values [34]

- Atomic force microscope: Bruker Dimension Icon with ScanAsyst

- E-beam lithography: Electron Beam Physical Vapor Deposition machine (E-Beam PVD system Polyteknik)

- Potentiostat: CH Instruments Electrochemical Workstation (CHI760E)

- Reference calibration electrode: Radiometer Analytical Ag/AgCl, model XR300, B20B300, batch 182B4-A10 in $1\,M\ Na_2SO_4$

- Reference electrode: eDAQ ET072-1 leak-less miniature Ag/AgCl electrode

- Sputter coater: Leica EM ACE600 Double sputter coater

- Solution water: milliQ water, $18.2\,M\Omega\,cm$

- Substrate support: p-type Silicon sample (Siegert Wafer)

A.3   Other AFM-analysis software

A key element in the mapping of nanomechanical properties using the AFM is the data analysis method. In addition to the method we present in section 5, here follows an assessment of other available software. Firstly, 'WXSM' [53] claims to provide many features, though specifies only adhesion mapping. It seems to be old and does not support Bruker data files, though it does support loading arbitrary data. Another tool, 'OpenFovea' [54], supports Bruker files, but only `.raw` files and not `.hsdc` files. It allows mapping of stiffness tomography, unbinding and the Young's modulus. However, its website is unreachable. Yet another free tool is 'FC_analysis' [55], which can map

Young's modulus, elasticity and stiffness and contains contact mechanics models. It can only read `.txt` files with F–z curves. This makes this tool applicable to different AFM systems, but requires extra processing steps, and costs more memory.

Finally, Gwyddion [56] can execute most aspects of AFM data processing, and recently introduced support for force–distance curves. It includes several contact mechanics models and supports many file formats, though not `.hsdc` files. However, the software is open source, and contrary to the earlier mentioned tools actively maintained and well documented. This makes it practical to write an extension for `.hsdc` files.

There is also suitable commercial software, such as SPIP and the Bruker QNM module for NanoScope. The latter supports real-time mapping of DMT modulus, adhesion, peak force, dissipation and deformation. Because it is made by the manufacturer of the AFM we used, it works for `.hsdc` file but also provides data formats more suitable for force maps.

A.4   Data sets

For reference, table 4, shows the experimental AFM and electrochemistry parameters of all normal pulse voltammetry datasets.

Dataset	Date	Tip	x_{scan} (nm)	PFA (nm)	k (N/m)	V_{RE} (mV)
NailPolish_Gold_8jan	13-02-2020	Scanasyst Fluid	1000	30	0.929	98
Sputter_Gold_incr	20-03-2020	Scanasyst Fluid	1000	30	1.542	150
Sputter_Gold_decr	20-03-2020	Scanasyst Fluid	1000	30	1.542	150
Sputter_Gold_zoom	20-03-2020	Scanasyst Fluid	1000	30	1.542	150
Sputter_Gold_spot	20-03-2020	Scanasyst Fluid	10	30	1.542	150
Wax_Gold_Ti_May	20-05-2020	Scanasyst Fluid	10	60	1.37	113
Wax_Gold_Ti_June	04-06-2020	Scanasyst Fluid	10	60	1.41	159

Table 4 – All measurement series used for normal pulse voltammetry, where x_{scan} is the scan size, PFA means peak force amplitude, k is the spring constant of the cantilever, and V_{RE} is the potential of the reference electrode vs. Ag/AgCl.

A.5   Extra figures

In the following part extra figures of the results of the experiments are shown.
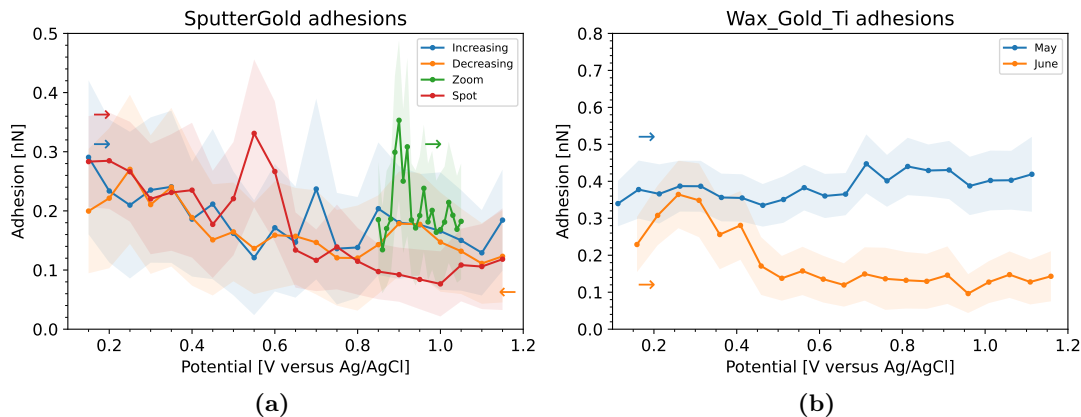
Figure 41 – Combined adhesions for multiple measurements on one sample. Shown are the samples (a) SputterGold, (b) WaxGoldTi.
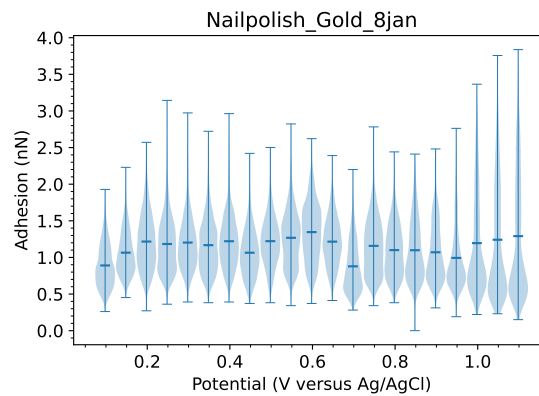
Figure 42 – Violin plot of adhesion versus potential for sample Nailpolish Gold 8jan.

A.6   Code

The figures in this thesis were made using Python scripts. Two scripts for reading the data files are listed below. The other twelve code files can be provided by the author upon request.

Listing 1 – code/hsdc_parameter_reader.py

```python
''' (c) Jim Carstens @ AMOLF 2020
Extracts all scan parameters from a Bruker .hsdc file
'''
import glob


def set_dict_value(d, line, quantity):
    '''Puts the quantity of line in dictionary'''
    if line.startswith(quantity):
        quantity = quantity[1:-1]
        value = line.split(':')[-1].strip().split()
        if len(value) > 1:
            if quantity == 'High Speed Data Type':
                value = value[0] + value[1]
            else:
                value = value[-2]
        else:
            value = value[0]
        if quantity in d:
            d[f'{quantity}_2'] = value
        else:
            d[quantity] = value

def clean_dict_values(d):
    '''Cleans the line name from .hsdc file in to dict key'''
    d['Scan Size'] = float(d['Scan Size'])  # nm
    d['Peak Force Amplitude'] = 1e-9 * float(d['Peak Force Amplitude'])  # m
    d['@Sens. ForceDeflSens'] = 1e-9 * float(d['@Sens. ForceDeflSens'])  # nN/V
    d['@2:SoftHarmoniXSetpoint'] = float(d['@2:SoftHarmoniXSetpoint'])  # V
    d['peak_force_frequency'] = 1e3 * float(d['@2:DriveFrequency3SoftHarmoniX'])
        # Hz
    d['Hsdc Duration'] = 1e-3 * float(d['Hsdc Duration'])  # s
    d['Data length_2'] = int(d['Data length_2'])  # bytes
    d['Tip Velocity'] = 1e3 * float(d['Tip Velocity'])  # nm/s

    if d['High Speed Data Type'] == 'DeflectionError':
        d['Data offset def'] = int(d.pop('Data offset'))  # bytes
        d['Hard Scale def'] = float(d.pop('High Speed Data Hard Scale'))  # V
        d['Soft Scale def'] = 1e-9 * float(d.pop('High Speed Data Soft Scale'))
            # m/V
    if d['High Speed Data Type'] == 'Height':
```

```
40          d['Data offset height'] = int(d.pop('Data offset'))  # bytes
41          d['Hard Scale height'] = float(d.pop('High Speed Data Hard Scale'))  # V
42          d['Soft Scale height'] = 1e-9 * float(d.pop('High Speed Data Soft Scale')
                )  # m/V
43      if d['High Speed Data Type'] == 'HeightSensor':
44          d['Data offset hsensor'] = int(d.pop('Data offset'))  # bytes
45          d['Hard Scale hsensor'] = float(d.pop('High Speed Data Hard Scale'))  # V
46          d['Soft Scale hsensor'] = 1e-9 * float(d.pop('High Speed Data Soft Scale'
                ))  # m/V

48      if d['High Speed Data Type_2'] == 'DeflectionError':
49          d['Data offset def'] = int(d.pop('Data offset_2'))  # bytes
50          d['Hard Scale def'] = float(d.pop('High Speed Data Hard Scale_2'))  # V
51          d['Soft Scale def'] = 1e-9 * float(d.pop('High Speed Data Soft Scale_2'))
                 # m/V
52      if d['High Speed Data Type_2'] == 'Height':
53          d['Data offset height'] = int(d.pop('Data offset_2'))  # bytes
54          d['Hard Scale height'] = float(d.pop('High Speed Data Hard Scale_2'))  #
                V
55          d['Soft Scale height'] = 1e-9 * float(d.pop('High Speed Data Soft Scale_2
                '))  # m/V
56      if d['High Speed Data Type_2'] == 'HeightSensor':
57          d['Data offset hsensor'] = int(d.pop('Data offset_2'))  # bytes
58          d['Hard Scale hsensor'] = float(d.pop('High Speed Data Hard Scale_2'))  #
                V
59          d['Soft Scale hsensor'] = 1e-9 * float(d.pop('High Speed Data Soft
                Scale_2'))  # m/V



63  def get_sync_distance(hsdc_file):
64      '''Reads the sync distance from a .hsdc'''
65      with open(hsdc_file, encoding="ansi") as f:
66          current_line = f.readline()
67          while not current_line.startswith('\\Sync Distance:'):
68              current_line = f.readline()
69      return float(current_line.split(':')[-1].strip())


72  def init_hsdc_params(hsdc_file):
73      '''Used as module, reads .hsdc, puts params in, returns hsdc_params'''
74      hsdc_params = {}
75      file_name = hsdc_file.split('\\')[-1].replace('.hsdc', '')
76      with open(hsdc_file, encoding="ansi") as f:
77          print(f'## Reading .HSDC parameters from {file_name}')
78          current_line = f.readline()
79          while current_line != '\\*File list end\n':
80              current_line = f.readline()
81              quantities = ['\\Date:',
82                            '\\Scan Size:',
83                            '\\Sync Distance:',
84                            '\\Peak Force Amplitude:',
85                            '\\@Sens. ForceDeflSens:',
86                            '\\@2:SoftHarmoniXSetpoint:',
87                            '\\@2:DriveFrequency3SoftHarmoniX:',
88                            '\\Hsdc Duration:',
89                            '\\Data offset:',
90                            '\\Data length:',
91                            '\\Tip Velocity:',
92                            '\\High Speed Data Type:',
93                            '\\High Speed Data Hard Scale:',
94                            '\\High Speed Data Soft Scale:']
95              for qty in quantities:
96                  set_dict_value(hsdc_params, current_line, qty)
97      clean_dict_values(hsdc_params)
98      return hsdc_params
```

```
99
100
101  def main():
102      '''Contains tests of the functions'''
103      directory = '../../..'
104      file_list = glob.glob(f"{directory}/HSDC*.hsdc")
105      file = file_list[0]
106      hsdc_params = init_hsdc_params(file)
107
108      for qty, val in hsdc_params.items():
109          print(qty, val, sep='\t')
110
111  if __name__ == "__main__":
112      main()
```

Listing 2 – code/module_file_reading.py

```
1   ''' (c) Jim Carstens @ AMOLF 2020
2   Contains helper functions for reading data files
3   '''
4   import os
5   import pandas as pd
6
7   def filename_to_voltage_string(filename):
8       ''' Removes the full path, extension, and only select the value hsdc_
            {value}_etc
9       Remove the directory, go from full path to only filename
10      '''
11      voltage_string = filename.split('\\')[-1]
12      # Only take the part containing the voltage
13      voltage_string = voltage_string.split('_')[1].split('.')[0]
14      if voltage_string[-1] == 'V':
15          return voltage_string[:-1]
16      return voltage_string
17
18  def voltage_string_to_float(filename):
19      '''Converts the format 'm9p9' to -9.9'''
20      new_string = ''
21      for i in filename:
22          if i == 'm':
23              new_string += '-'
24          elif i == 'p':
25              new_string += '.'
26          else:
27              new_string += i
28      return float(new_string)  # No error checking occurs here
29
30  def skip_to(fle, line, **kwargs):
31      '''Reads a file starting from a line that starts with line,
32      return a pandas Df'''
33      if os.stat(fle).st_size == 0:
34          raise ValueError("File is empty")
35      with open(fle, encoding="utf-8") as f:
36          pos = 0
37          cur_line = f.readline()
38          while not cur_line.startswith(line):
39              pos = f.tell()
40              cur_line = f.readline()
41          f.seek(pos)
42          return pd.read_csv(f, **kwargs)
43
44  def get_scan_rate(fle):
45      '''Takes a file and returns its scan rate in V/s'''
46      if os.stat(fle).st_size == 0:
47          raise ValueError("File is empty")
48      with open(fle, encoding="utf-8") as f:
```

```
49          cur_line = f.readline()
50          while not cur_line.startswith('Scan Rate (V/s)'):
51              cur_line = f.readline()
52          return float(cur_line.split(' ')[-1].split('\n')[0])
```

Example of a potentiostat data text file:

```
1   Open Circuit Potential - Time
2   File: ocp1
3   Data Source:  Experiment
4   Instrument Model:  CHI760E
5   Header:
6   Note:
7
8   Run Time (sec) = 1e+3
9
10  Time/sec, Potential/V
11
12  1.000e-1, -1.231e-1
13  2.000e-1, -1.216e-1
```

A.7   Acronyms

- AFM - atomic force microscope

- CE - counter electrode

- CV - cyclic voltammetry

- DLVO - Derjaguin–Landau–Verwey–Overbeek

- DMT - Derjaguin–Muller–Toropov

- EC - electrochemical

- EDL - electric double-layer

- GCS - Gouy–Chapman–Stern

- HSDC - high speed data capture

- JKR - Johnson–Kendall–Roberts

- KPFM - kelvin probe force microscopy

- NPV - normal pulse voltammetry

- OCP - open circuit potential

- PB - Poisson–Boltzmann

- PFA - peak force amplitude

- PFF - peak force frequency

- PFT - peak force tapping

- RE - reference electrode

- SCV - staircase voltammetry

- SECM - scanning electrochemical microscopy

- SPM - scanning probe microscopy

- WE - working electrode

- vdW - van der Waals

References

1. Wolfschmidt, H. *et al.* STM, SECPM, AFM and Electrochemistry on Single Crystalline Surfaces. *Materials* **3,** 4196–4213. doi:`10.3390/ma3084196` (2010).

2. Wang, R. *et al.* Operando Atomic Force Microscopy Reveals Mechanics of Structural Water Driven Battery-to-Pseudocapacitor Transition. *ACS Nano* **12,** 6032–6039. doi:`10.1021/acsnano.8b02273` (2018).

3. Ardo, S. *et al.* Pathways to Electrochemical Solar-Hydrogen Technologies. *Energy & Environmental Science* **11,** 2768–2783. doi:`10.1039/C7EE03639F` (2018).

4. Futscher, M. H., Gangishetty, M. K., Congreve, D. N. & Ehrler, B. Quantifying Mobile Ions and Electronic Defects in Perovskite-Based Devices with Temperature-Dependent Capacitance Measurements: Frequency vs Time Domain. *The Journal of Chemical Physics* **152,** 044202. doi:`10.1063/1.5132754` (31st Jan. 2020).

5. Bard, A. J. & Faulkner, L. R. *Electrochemical Methods: Fundamentals and Applications* 2nd ed. ISBN: 978-0-471-04372-0 (Wiley, New York, 2001).

6. Ahmad, Z. in *Principles of Corrosion Engineering and Corrosion Control* 271–351 (Elsevier, 2006). ISBN: 978-0-7506-5924-6. doi:`10.1016/B978-075065924-6/50006-4`.

7. Zhu, J. *et al.* Direct Imaging of Highly Anisotropic Photogenerated Charge Separations on Different Facets of a Single BiVO$_4$ Photocatalyst. *Angewandte Chemie* **127,** 9239–9242. doi:`10.1002/ange.201504135` (2015).

8. Li, H. *et al.* Kinetic Study of Hydrogen Evolution Reaction over Strained MoS$_2$ with Sulfur Vacancies Using Scanning Electrochemical Microscopy. *Journal of the American Chemical Society* **138,** 5123–5129. doi:`10.1021/jacs.6b01377` (20th Apr. 2016).

9. Yang, X.-F. *et al.* Single-Atom Catalysts: A New Frontier in Heterogeneous Catalysis. *Accounts of Chemical Research* **46,** 1740–1748. doi:`10.1021/ar300361m` (20th Aug. 2013).

10. Giannakakis, G., Flytzani-Stephanopoulos, M. & Sykes, E. C. H. Single-Atom Alloys as a Reductionist Approach to the Rational Design of Heterogeneous Catalysts. *Accounts of Chemical Research* **52,** 237–247. doi:`10.1021/acs.accounts.8b00490` (15th Jan. 2019).

11. Knittel, P., Mizaikoff, B. & Kranz, C. Simultaneous Nanomechanical and Electrochemical Mapping: Combining Peak Force Tapping Atomic Force Microscopy with Scanning Electrochemical Microscopy. *Analytical Chemistry* **88,** 6174–6178. doi:`10.1021/acs.analchem.6b01086` (21st June 2016).

12. Nellist, M. R. *et al.* Atomic Force Microscopy with Nanoelectrode Tips for High Resolution Electrochemical, Nanoadhesion and Nanoelectrical Imaging. *Nanotechnology* **28,** 095711. doi:`10.1088/1361-6528/aa5839` (3rd Mar. 2017).

13. Liu, F., Klaassen, A., Zhao, C., Mugele, F. & Van Den Ende, D. Electroviscous Dissipation in Aqueous Electrolyte Films with Overlapping Electric Double Layers. *Journal of Physical Chemistry B* **122,** 933–946. doi:`10.1021/acs.jpcb.7b07019` (2018).

14. Clark, N., Oikonomou, A. & Vijayaraghavan, A. Ultrafast Quantitative Nanomechanical Mapping of Suspended Graphene. *physica status solidi (b)* **250,** 2672–2677. doi:`10.1002/pssb.201300137` (2013).

15. Bruker Corporation. *Peak Force QNM* (2011), 95.

16. Xu, K. *et al.* Recent Development of PeakForce Tapping Mode Atomic Force Microscopy and Its Applications on Nanoscience. *Nanotechnology Reviews* **7,** 605–621. doi:`10.1515/ntrev-2018-0086` (19th Dec. 2018).

17.   Shi, X., Qing, W., Marhaba, T. & Zhang, W. Atomic Force Microscopy - Scanning Electrochemical Microscopy (AFM-SECM) for Nanoscale Topographical and Electrochemical Characterization: Principles, Applications and Perspectives. *Electrochimica Acta* **332,** 135472. doi:`10.1016/j.electacta.2019.135472` (Feb. 2020).

18.   Bruker Corporation. An Introduction to AFM-Based Scanning Electrochemical Microscopy: PeakForce SECM, 11 (2017).

19.   Nonnenmacher, M., O'Boyle, M. P. & Wickramasinghe, H. K. Kelvin Probe Force Microscopy. *Applied Physics Letters* **58,** 2921–2923. doi:`10.1063/1.105227` (24th June 1991).

20.   Collins, L. *et al.* Probing Charge Screening Dynamics and Electrochemical Processes at the Solid-Liquid Interface with Electrochemical Force Microscopy. *Nature Communications* **5,** 1–8. doi:`10.1038/ncomms4871` (May 2014).

21.   Hirata, K. *et al.* Visualizing Charges Accumulated in an Electric Double Layer by Three-Dimensional Open-Loop Electric Potential Microscopy. *Nanoscale* **10,** 14736–14746. doi:`10.1039/c8nr03600d` (2018).

22.   Voïtchovsky, K., Kuna, J. J., Contera, S. A., Tosatti, E. & Stellacci, F. Direct mapping of the solid–liquid adhesion energy with subnanometre resolution. *Nature Nanotechnology* **5,** 401–405. doi:`10.1038/nnano.2010.67` (Apr. 2010).

23.   Compton, R. G. & Banks, C. E. *Understanding Voltammetry* 3rd ed., 375–377. ISBN: 978-1786345264. doi:`10.1142/q0155` (World Scientific (Europe), Aug. 2018).

24.   Van Roij, R. *Soft Condensed Matter Theory* Reader (Institute for Theoretical Physics, Utrecht University, Feb. 2019), 83–84.

25.   Archer, D. G. & Wang, P. The Dielectric Constant of Water and Debye-Hückel Limiting Law Slopes. *Journal of Physical and Chemical Reference Data* **19,** 371–411. doi:`10.1063/1.555853` (Mar. 1990).

26.   Helmholtz, H. v. Ueber einige Gesetze der Vertheilung elektrischer Ströme in körperlichen Leitern, mit Anwendung auf die thierisch-elektrischen Versuche (Schluss). *Annalen der Physik* **165,** 353–377. doi:`10.1002/andp.18531650702` (1853).

27.   Israelachvili, J. N. *Intermolecular and Surface Forces* 3rd ed. ISBN: 9780123751829. doi:`10.1016/c2009-0-21560-1` (Elsevier, 2011).

28.   Verwey, E. J. W., Overbeek, J. T. G. & Van Nes, K. *Theory of the stability of lyophobic colloids: The interaction of sol particles having an electric double layer* `https://digital.library.cornell.edu/catalog/chla2906086` (Elsevier Publishing Company, Amsterdam, 1948).

29.   Hook, J. R. & Hall, H. E. *Solid State Physics* 2nd ed., 28–29. 474 pp. ISBN: 978-0-471-92805-8 (Wiley, Chichester; New York, 1991).

30.   Cappella, B. in. *Mechanical Properties of Polymers Measured through AFM Force-Distance Curves* 3–66 (Springer International Publishing, Cham, 2016). ISBN: 978-3-319-29457-5. doi:`10.1007/978-3-319-29459-9_1`.

31.   Chen, G. *Nanoscale energy transport and conversion: A parallel treatment of electrons, molecules, phonons, and photons* 416–421. ISBN: 0-19-515942-X (Oxford University Press, 2005).

32.   Leite, F. L., Bueno, C. C., Da Róz, A. L., Ziemath, E. C. & Oliveira, O. N. Theoretical models for surface forces and adhesion and their measurement using Atomic Force Microscopy. *International Journal of Molecular Sciences* **13,** 12773–12856. doi:`10.3390/ijms131012773` (Oct. 2012).

33.   Ricci, M. *Characterization of Solid-Liquid Interfaces with High-Resolution Atomic Force Microscopy* (EPFL, Lausanne, 2015). 192 pp. doi:`10.5075/epfl-thesis-6568`.

34. Bruker Corporation. *ScanAsyst-Fluid – Bruker AFM Probes* `https://www.brukerafmprobes.com/p-3727-scanasyst-fluid.aspx` (2020).

35. Butt, H.-J. Electrostatic Interaction in Scanning Probe Microscopy When Imaging in Electrolyte Solutions. *Nanotechnology* **3,** 60–68. doi:`10.1088/0957-4484/3/2/003` (1st Apr. 1992).

36. Siretanu, I. *et al.* Direct observation of ionic structure at solid-liquid interfaces: A deep look into the Stern Layer. *Scientific Reports* **4,** 4956. doi:`10.1038/srep04956` (May 2014).

37. Zhao, C., Ebeling, D., Siretanu, I., Van Den Ende, D. & Mugele, F. Extracting Local Surface Charges and Charge Regulation Behavior from Atomic Force Microscopy Measurements at Heterogeneous Solid-Electrolyte Interfaces. *Nanoscale* **7,** 16298–16311. doi:`10.1039/c5nr05261k` (2015).

38. Johnson, K. L., Kendall, K., Roberts, A. D. & Tabor, D. Surface Energy and the Contact of Elastic Solids. *Proceedings of the Royal Society of London. A. Mathematical and Physical Sciences* **324,** 301–313. doi:`10.1098/rspa.1971.0141` (8th Sept. 1971).

39. Serafin, J. M., Hsieh, S.-J., Monahan, J. & Gewirth, A. A. Potential Dependent Adhesion Forces on Bare and Underpotential Deposition Modified Electrode Surfaces. *The Journal of Physical Chemistry B* **102,** 10027–10033. doi:`10.1021/jp982881q` (1st Dec. 1998).

40. Merrill, D. R., Stefan, I. C., Scherson, D. A. & Mortimer, J. T. Electrochemistry of Gold in Aqueous Sulfuric Acid Solutions under Neural Stimulation Conditions. *Journal of The Electrochemical Society* **152,** E212. doi:`10.1149/1.1921850` (2005).

41. Lipkowski, J., Shi, Z., Chen, A., Pettinger, B. & Bilger, C. Ionic Adsorption at the Au(111) Electrode. *Electrochimica Acta* **43,** 2875–2888. doi:`10.1016/S0013-4686(98)00028-0` (June 1998).

42. Kondo, T. *et al.* Structure of Au(111) and Au(100) Single-Crystal Electrode Surfaces at Various Potentials in Sulfuric Acid Solution Determined by in Situ Surface X-ray Scattering. *Journal of Physical Chemistry C* **111,** 13197–13204. doi:`10.1021/jp072601j` (2007).

43. Rand, D. & Woods, R. A study of the dissolution of platinum, palladium, rhodium and gold electrodes in 1 M sulphuric acid by cyclic voltammetry. *Journal of Electroanalytical Chemistry and Interfacial Electrochemistry* **35,** 209–218. doi:`10.1016/s0022-0728(72)80308-5` (Mar. 1972).

44. Ma, W. *et al.* Investigating Electron-Transfer Processes Using a Biomimetic Hybrid Bilayer Membrane System. *Nature Protocols* **8,** 439–450. doi:`10.1038/nprot.2013.007` (Mar. 2013).

45. Valenti, M. *et al.* Suppressing H_2 Evolution and Promoting Selective CO_2 Electroreduction to CO at Low Overpotentials by Alloying Au with Pd. *ACS Catalysis* **9,** 3527–3536. doi:`10.1021/acscatal.8b04604` (Mar. 2019).

46. Elgrishi, N. *et al.* A practical beginner's guide to Cyclic Voltammetry. *Journal of Chemical Education* **95,** 197–206. doi:`10.1021/acs.jchemed.7b00361` (2018).

47. NISE Network. *Scientific Image - Atomic Force Microscope Illustration* `https://www.nisenet.org/catalog/scientific-image-atomic-force-microscope-illustration` (2019).

48. CH Instruments. *Model 700E Series Electrochemical Analyzer/Workstation User Manual* (Nov. 2012).

49. The SciPy community. *SciPy v1.6.3 Reference Guide – scipy.signal.find_peaks* `https://docs.scipy.org/doc/scipy/reference/generated/scipy.signal.find_peaks.html` (2020).

50. Aarts, M. & Alarcón-Lladó, E. Directed nanoscale metal deposition by the local perturbation of charge screening at the solid–liquid interface. *Nanoscale* **11,** 18619–18627. doi:`10.1039/c9nr05574f` (2019).

51. Nečas, D., Valtr, M. & Klapetek, P. How Levelling and Scan Line Corrections Ruin Roughness Measurement and How to Prevent It. *Scientific Reports* **10,** 15294. doi:`10.1038/s41598-020-72171-8` (Dec. 2020).

52. Sader, J. E. *et al.* A Virtual Instrument to Standardise the Calibration of Atomic Force Microscope Cantilevers. *Review of Scientific Instruments* **87,** 093711. doi:`10.1063/1.4962866` (Sept. 2016).

53. Horcas, I. *et al.* WSXM: A Software for Scanning Probe Microscopy and a Tool for Nanotechnology. *Review of Scientific Instruments* **78.** doi:`10.1063/1.2432410` (2007).

54. Roduit, C. *et al.* OpenFovea: Open-source AFM Data Processing Software. *Nature Methods* **9,** 774–775. doi:`10.1038/nmeth.2112` (2012).

55. Dinarelli, S., Girasole, M. & Longo, G. FC_analysis: A Tool for Investigating Atomic Force Microscopy Maps of Force Curves. *BMC Bioinformatics* **19,** 258. doi:`10.1186/s12859-018-2265-4` (Dec. 2018).

56. Nečas, D. & Klapetek, P. Gwyddion: An Open-Source Software for SPM Data Analysis. *Open Physics* **10.** doi:`10.2478/s11534-011-0096-2` (1st Jan. 2012).